BEHAVIOR OF SPHERICAL PARTICLES AT LOW REYNOLDS NUMBERS IN A FLUCTUATING TRANSLATIONAL FLOW

Thesis by

Murray Keith Hill

In Partial Fulfillment of the Requirements

for the Degree of

Doctor of Philosophy

California Institute of Technology

Pasadena, California

1973

(Submitted September 13, 1972)

ACKNOWLEDGMENTS

The author would like to thank his research advisor, Professor Zukoski, for his guidance and encouragement at all times.

The author would also like to express his appreciation for the many helpful suggestions from Professors F. E. Marble and W. D. Rannie.

The author would like to thank Imperial Oil of Canada, Ltd. for providing a Graduate Research Fellowship during the first three years of the author's stay at the Institute. Thanks are also due the California Institute of Technology for tuition scholarships in all years and a research assistantship during the author's final year at the Institute.

Partial financial support for this research from the Aerospace Research Laboratories (AFSC), Wright-Patterson Air Force Base, is also gratefully acknowledged.

Special thanks are due Mr. F. T. Linton for his great help in the experimental work and for his careful preparation of the figures. Thanks are also due Mrs. Linda Palmrose and Mrs. R. Duffy for their excellent typing of the manuscript.

Finally, the author would like to express his utmost thanks to his wife, whose assistance and support made this work possible.

ABSTRACT

The behavior of spheres in non-steady translational flow has been studied experimentally for values of Reynolds number from 0.2 to 3000. The aim of the work was to improve our qualitative understanding of particle transport in turbulent gaseous media, a process of extreme importance in power plants and energy transfer mechanisms.

Particles, subjected to sinusoidal oscillations parallel to the direction of steady translation, were found to have changes in average drag coefficient depending upon their translational Reynolds number, the density ratio, and the dimensionless frequency and amplitude of the oscillations. When the Reynolds number based on sphere diameter was less than 200, the oscillation had negligible effect on the average particle drag.

For Reynolds numbers exceeding 300, the coefficient of the mean drag was increased significantly in a particular frequency range. For example, at a Reynolds number of 3000, a 25 per cent increase in drag coefficient can be produced with an amplitude of oscillation of only 2 per cent of the sphere diameter, providing the frequency is near the frequency at which vortices would be shed in a steady flow at the mean speed. Flow visualization shows that over a wide range of frequencies, the vortex shedding frequency locks in to the oscillation frequency. Maximum effect at the natural frequency and lock-in show that a non-linear interaction between wake vortex shedding and the oscillation is responsible for the increase in drag.

LIST OF SYMBOLS

a: acceleration

A: amplitude of the fluid oscillation

A_p: amplitude of the relative motion between the particle and the fluid

B: time dependent drag force

C_D: drag coefficient = $\text{Drag} / (\frac{1}{2} \rho V^2 \text{Area})$

C_{D_o}: drag coefficient of the sphere at terminal velocity in a quiescent fluid.

$C_{\overline{D}}$: coefficient of the mean drag, $\overline{D} / (\frac{1}{2} \rho \overline{V}^2 \text{Area})$

C_H: coefficient of the time dependent drag term

C_M: added mass coefficient

d: sphere diameter

D: drag force

$\overline{D}$: mean drag force

f: frequency of the fluid oscillation

f_{ST_o}: vortex shedding frequency for a sphere of diameter d at velocity U_o and Reynolds number Re_o

f_{ST}: vortex shedding frequency for a sphere of diameter d at a steady velocity U and Reynolds number Re

g: acceleration due to gravity

m_s: mass of the sphere

m: mass of the fluid displaced by the sphere

r: radius of the sphere

Re: Reynolds number = Vd/ν; also the Reynolds number corresponding to the mean speed of the sphere in an oscillating fluid

Re_o: terminal Reynolds number of the sphere in a quiescent fluid, $U_o d/\nu$

t: time

U: velocity of the sphere in an oscillating fluid

U_o: terminal velocity of the sphere in a quiescent fluid

$\Delta\overline{U}$: $U_o - \overline{U}$

V: fluid velocity

$\dot{V}$: fluid acceleration

V_{rel}: relative velocity between the sphere and the fluid

x: position

δ: boundary layer thickness

μ: absolute viscosity of the fluid

ν: kinematic viscosity of the fluid

ρ: density of the fluid

ρ_s: density of the sphere

ω: angular frequency of the fluid oscillation

$\overline{(\ )}$: denotes time-averaged quantity

LIST OF FIGURES

TABLE OF CONTENTS

TABLE OF CONTENTS
(Continued)

INTRODUCTION

The two outstanding fundamental problems that limit the technological development of dusty gas dynamics are: (1) the near-field interaction between solid particles or between a particle and a solid surface, and (2) the behavior of solid particles in a turbulent medium.

The first of these has been considered in some detail analytically[1] and experimentally[2], utilizing a fluidized bed in the study of interactions with large volume fractions of solid particles.

The second of these problems, the movement of solid particles in a turbulent flow field, has been considered by some investigators[3, 4], to concern a problem of particle drag coefficient as affected by the stream turbulence level. In the case of micron-sized particles, where the particle size is small compared with the turbulence macroscale, it seems doubtful that this picture is an appropriate one.

On the other hand, other investigators -- notably Tchen[5], Corrsin and Lumley[6], and Lumley[7] -- consider the migration of particles in a turbulent field possessing certain statistical properties. These efforts come much closer to the problem of technical interest and are limited largely by the turbulence statistics and the general complexity of the calculation. This work does not, however, account for the effects which a dense cloud of particles would have upon the turbulence structure. It is to be

expected that, depending upon the particle size, a selected portion of the turbulence spectrum would be altered by particle attenuation similar to the well-known selective attenuation of acoustic fields by particle clouds.

Calculations of the particle transport by a turbulent field have been carried out using essentially a modification to the Stokes law which accounts, in a certain measure, for linear non-steady effects. This is certainly an understandable assumption since this improves, somewhat, its analytical tractability. However, in many cases of technological interest, the Reynolds number of the particle motion relative to the fluid is large enough so that this relatively simple law is inapplicable. The anomalous, low drag coefficients observed in refs. 3 and 4 at Reynolds numbers between 10 and 10^3 were attributed in ref. 4 to premature transition on the sphere induced by the high level of stream turbulence. It would seem that a more acceptable and profitable approach is to recognize that these small spheres exist in a severly non-steady flow field, in which relative velocities may be reversed by fluctuations, and to understand something of their behavior under these circumstances.

The anomalous behavior of spheres moving freely in fluids is a matter of historical record as well as one of continuing research interest, refs. 8-15. There are obvious changes in the mode of flow in certain ranges of Reynolds number that involve vortex shedding, asymmetric forces, and, in general, significant departures from mean values frequently quoted. In the turbulent

transport problem the situation is further complicated by the strongly non-steady flow to which the particle is subjected.

The current work was stimulated by an effort to understand the measurements of refs. 3, 4, 18-20 on the basis of the forces acting on a sphere in severly non-steady flow rather than on the basis of turbulent boundary layer transitions on a sphere at Reynolds number of the order 10^2. To accomplish this, it appeared necessary to measure the sphere response to fluctuations in translational velocity which were of the same magnitude as the mean translational velocity. This is a very difficult experimental problem (e.g. ref. 37) in the Reynolds number range of interest.

The technique that has been adopted in the present investigation was suggested by some processes in the chemical industry and its use in refs. 14 and 17 to study problems related to the present one. In our adaptation, we utilize a large, vertical, rigid tube, completely filled with liquid and mounted upon a movable table which oscillates the tube along its axis in a vertical direction. This shaker is capable of providing large amplitude oscillation over a wide frequency range. Spheres, of suitable size and material, are released at the top of the tube and fall, under gravitational influence, through the oscillating liquid. In this manner, because the liquid is effectively incompressible, the experiment duplicates, quite reasonably, the free motions of particles through an oscillating fluid field of large scale and

permits drag measurements based upon transit time for a fixed distance.

It is important to point out that the experiment does not duplicate the motion of a particle through a turbulent field, not only because of the single frequency present and the one-dimensionality of the disturbance, but because the length scale of the fluctuating field is effectively infinite. It does, however, suggest modifications to the particle drag law which shed considerable light on the behavior of non-streamlined bodies in unsteady flows.

II. BACKGROUND

Although the flow past spheres has been studied since the time of Newton, the complexity of the flow is such that many features are still not well understood. In a series of articles, Torobin and Gauvin[21] have presented a thorough review of the published work up to 1959. Subsequent work has shed such light on the subject, particularly on the physical description of the flow in the vortex shedding regime, that it is worthwhile to present a brief description of the various steady flow regimes as well as some recent results on unsteady flows past bluff (non-streamlined) bodies.

A. Sphere Steady Flow Regimes

In the case of uniform steady flow past a fixed body, the flow field can be characterized by the Reynolds number, defined as

$$Re = Vd/\nu \quad .$$

The drag on such a body, when non-dimensionalized by the dynamic head times the frontal area can be shown to be simply a function of Reynolds number and the shape of the body.

A plot of drag coefficient versus Reynolds number for steady sphere flow is shown in figure 1 along with sketches of the wake in several regimes. Following is a description of these flow regimes.

1. $0 < Re < 0.1$ (Stokes Regime). For this Reynolds number range, the flow has been studied extensively analytically and is well understood. The fluid flows around the sphere without separation and the flow field is symmetric fore and aft of the sphere as well as being axisymmetric. The fore, aft symmetry follows from the complete neglect of the inertia terms in the equation of motion and implies that

the drag on the sphere is two-thirds shear drag and one-third pressure drag. The drag is given by ($6\pi\mu r V$), which, when non-dimensionalized, gives

$$C_D = D / \tfrac{1}{2}\rho V^2 \pi r^2 = 24/Re$$

2. $0.1 < Re < 20$. The mathematical description of the flow becomes increasingly difficult as the inertia of the fluid becomes more important. As the Reynolds number increases, the flow loses its fore, aft symmetry and the drag begins to reflect the increase in the non-symmetrical pressure distribution. The flow remains axisymmetric, however, and the fluid still negotiates the sphere without separation.

3. $20 < Re < 130$. Here, the flow separates from the sphere, and a stable, axisymmetric, vortex-like wake forms behind the sphere. The size of the vortex and the separation angle have been recorded carefully by Taneda[22] and these are shown in figure 2. It can be seen that a simple extension of these curves to their zero values would give conflicting values of the Reynolds number at which separation first occurs. Nisi and Porter[23], Magarvey and Bishop[8], and Rimon and Cheng[24] claim that separation occurs near Re = 10, while Masliyah and Epstein[25], Dennis and Walker[26], Jensen[27], Masliyah[28], and Pruppacher, et al.[29] report the boundary as closer to Re = 20. Masliyah and Epstein[25] legitimately object to Nisi and Porter's results on the basis of their determination of the freestream Reynolds number through the average velocity, in what is most likely a fully-developed channel flow. The transition Reynolds number found by

Magarvey and Bishop is also suspect due to their use of liquid droplets as particles -- the different boundary conditions at the surface could conceivably have a considerable effect on a transition number. The bulk of the experimental and numerical work shows that separation occurs near Re = 20 and that the steady wake vortex grows as the log of the Reynolds number up to Re = 130.

4. $130 < Re < 210$. At Re = 130 Taneda[22] reports that the far end of the vortex becomes unstable and the length of the vortex oscillates in time. There is always a question of whether or not the mechanism used to support the sphere has any influence in studies of this kind, particularly when the support must enter at the side of the sphere. Taneda reports, however, that there were no noticeable changes when the size of the support wire changed.

5. $210 < Re < 290$. In this range, the vortex loses its axisymmetry and a double thread wake is shed. Because of the asymmetry of the vortex, lift is generated on the sphere, and a sphere falling or rising under the influence of gravity will no longer fall in a vertical trajectory. The transition Reynolds numbers 210 and 290 have been measured for droplets, from which dye was continuously scrubbed by the surrounding liquid to reveal the wake structure, by Magarvey and Bishop[8], to within a spread of ± 10 in Reynolds number. They have been verified by Goldburg and Florsheim[31] using dye-coated solid spheres. In each case, the exact transition number might be slightly different than that for a solid sphere. Near Re = 270 the wake begins to show some instability. The double thread wake is wavy and shows a definite rotation about the axis of fall. Excellent pictures of

wakes of droplets for $170 < Re < 370$ are shown by Magarvey and Bishop[32].

6. $290 < Re < 700$. In this Reynolds number range, the wake is unstable and regular vortex shedding occurs. During this cyclic process, the ring vortex behind the sphere is at some time distorted so that it is largest at one position and smallest at a diametrically opposite position. The enlarged portion of the ring stretches into a loop which begins to move downstream, depleting the wake on this side of the sphere. As the vortex builds up again, it is the opposite side that is the largest, and a loop pulls away from that side. This process continues, alternating from side to side, but the plane in which this happens rotates, at a frequency much smaller than the vortex-shedding frequency. That is, the vortex shedding precesses around the vortex ring. This precession probably accounts for the helical motion of a sphere in free fall in this Reynolds number range.

Goldburg and Florsheim[31] have investigated the frequency of vortex shedding from solid spheres in free fall in this range by photographing the wake of dye-coated spheres. They find it to fit the relationship

$$f_{ST}\, d/V = 0.387\,(1 - 270/Re) \qquad (1)$$

7. $700 < Re < 300,000$. Above Re = 700, vortex shedding occurs with somewhat less regularity, and frequency measurements based on wake photographs are no longer possible, e.g. references 8, 31. However, Möller[33], who used a high-speed cinematography technique,

reports a Strouhal number of 0.4 (defined as in equation (1)) for $1500 < Re < 10,000$. He also reports a further wake unsteadiness at a much higher frequency. In some unpublished work, Kendall[14] measured fluctuations in the wake of a sphere two or three diameters downstream and found a Strouhal number of about 0.36 for Reynolds numbers up to 40,000. To our knowledge, no determination of shedding frequency for spheres has been made above 40,000.

Throughout these changes in wake structure the drag coefficient exhibits no sharp changes, and decreases smoothly to a nearly constant value of 0.4 from Re = 3,000 to Re = 10,000. In fact, the standard drag data are nicely fit in the range $0 < Re < 3000$ by a formula presented by Abraham[34]:

$$C_D = \frac{24}{(9.06)^2}\left[1 + \frac{9.06}{\sqrt{Re}}\right]^2 \qquad (2)$$

The drag coefficient rises from 0.4 at Re = 10,000 to about 0.48 at Re = 300,000.

As the Reynolds number increases, turbulent transition occurs on the separated shear layer closer to the point of laminar separation until, near Re = 300,000, the separated layer reattaches and turbulent separation occurs much further back on the sphere. The resulting narrowing of the wake and increased base pressure causes a dramatic drop in the drag coefficient from about 0.5 to about 0.15. The Reynolds number at which the drag coefficient is 0.3 is termed the upper critical Reynolds number. It is interesting that through all the changing wake phenomena, this is the only one which changes the

drag coefficient in a dramatic fashion.

8. Re > 300,000. Beyond 300,000 the point of turbulent separation shifts forward slightly and the drag coefficient shows a gradual increase. Willmarth and Enlow[11], investigating lift and moment fluctuations on a sphere at supercritical Reynolds number, found that the power spectrum of the lift showed no significant energy at any discrete frequency. Roos and Willmarth[13] have found, at lower Reynolds number, that fluctuating lift correlated with wake unsteadiness, so presumably the results of Willmarth and Enlow show that there is no tendency toward periodic shedding at supercritical Reynolds number. This is not the case in cylinder flow, where a discrete frequency is absent in the critical region but reappears at supercritical Reynolds number.

B. The Effect of Freestream Turbulence

An important consideration in sphere drag is the effect of freestream turbulence. Early research by Dryden, at al.[60] has shown that, in the critical regime, freestream turbulence can have a pronounced effect on sphere drag through its lowering of the Reynolds number at which turbulent reattachment occurs, higher turbulence levels corresponding to lower values of the critical Reynolds number. Torobin and Gauvin[4] and Clamen and Gauvin[20] have attempted to extend these results to much higher turbulence levels and lower Reynolds numbers through the use of a concurrent turbulent flow tunnel in which spheres are injected in the direction of the flow. Turbulence levels with respect to the slip velocity are as high as 35 per cent. Their

results show that for a particular turbulence level the drag decreases below the standard value, then increases to values above the standard, and finally decreases to the standard value as Reynolds number increases. They interpret this result as showing that turbulent reattachment is occurring, such that at a turbulence level of 35 per cent the critical Reynolds number is only 370. However, their method of drag measurement is highly suspect, as it involves double differentiation of only six position - time measurements to obtain acceleration data. Their work has not been verified in any independent experiment.

Zarin and Nicholls[12], using a turbulent-flow tunnel equipped with a magnetic balance, have measured sphere drag at considerably lower turbulence levels and found that sphere drag increases proportional to the turbulence level and increases with Reynolds number in the range $200 < Re < 800$. No changes were measured for $Re < 200$. They also found that when turbulent scales were the order of or smaller than the sphere diameter that there was a diameter effect; the drag increasing as the inverse of the sphere diameter. It is unfortunate that none of this work overlaps that of Torobin and Gauvin.

C. Drag in Unsteady Flow

In view of the complexity of the sphere flow field as a function of Reynolds number for steady flows, it is not surprising that the problem of a general unsteady flow has not been solved. Sphere flow in which the instantaneous Reynolds number is always in the Stokes range gives some insight. In this case, the equations of motion can be solved[61] to give an equation for the drag:

$$D = 6\pi\mu r V + \tfrac{1}{2}(\tfrac{4}{3}\pi r^3)\rho\dot{V} + 6r^2\sqrt{\pi\rho\mu}\int_{-\infty}^{t}\frac{1}{\sqrt{t-\tau}}\,\frac{dV}{d\tau}\,d\tau \qquad (3)$$

It can be seen that the drag depends not only on the instantaneous velocity and acceleration but indeed on the entire time history of the acceleration. This time history term is commonly called the Basset term and is usually denoted by $B(t)$.

It is to be expected that the drag at higher Reynolds numbers will depend on the complete time history of the acceleration, but not through the same functional dependence as in equation (3). This is evident from a comparison of high and low Reynolds number steady drag laws which show a dependence on V^2 and V, respectively. An examination of the Navier-Stokes equations can give some general information of when the acceleration will be important. The form of the dependence is, however, still unknown.

At low Reynolds numbers, if the forces due to the acceleration are the order of the forces due to the viscous shear, i.e., if

$$\rho\frac{\partial V}{\partial t} \sim \mu\frac{\partial^2 V}{\partial x^2}$$

or

$$ad^2/\nu V \sim 1 \qquad (4)$$

the acceleration, a, will be important. This parameter, $ad^2/\nu V$, also appears when the magnitude of the added mass term is compared with that of the steady drag term in equation (3), or when the magnitudes of the history term and the steady drag term are compared. Hence, $ad^2/\nu V$ is the pertinent parameter for low Reynolds numbers.

For high Reynolds number flows, the scale length for the diffusion of momentum is the boundary layer thickness rather than the diameter and condition (4) becomes

$$a\delta^2/\nu V \sim 1$$

Since

$$\delta/d = c/\sqrt{Re}$$

when the boundary layer is laminar, this condition reduces to:

$$ad/V^2 \sim 1 \qquad (5)$$

In the case of an oscillating flow this condition is equivalent to

$$fd/V \sim 1 \qquad (6)$$

The expectation is that, for arbitrary Reynolds number, if the appropriate condition (4), (5), or (6) is reached or exceeded, the instantaneous acceleration and its time history will affect the drag.

Because of the intractability of the theoretical problem at Reynolds numbers above unity, and the improbability of solving the complete problem experimentally, the approach has been to study experimentally various specific motions. The hope is that results so obtained may be applied to more general motions. These experiments on unsteady flows past bluff bodies can be divided into two main categories:

1. unidirectional acceleration
    a) impulsive start
    b) constant acceleration
    c) monatonic acceleration

2. oscillatory acceleration

   a) purely oscillatory motion

   b) oscillatory motion with a mean flow

A common procedure in 1. a) and 1. b) is to measure the drag force and wake properties and to correlate the dimensionless quantities with Reynolds number and dimensionless position or acceleration. Note that dimensional analysis implies that only one parameter in addition to the Reynolds number is needed in either of these two cases.

A monatonic acceleration, for example the acceleration of a particle up to terminal velocity in free fall, is a more complicated situation. The properties of the flow depend, in general, on the entire time history of the motion, or equivalently, on the dimensionless velocity and all its (dimensionless) derivatives. Frequently, the drag forces are measured or inferred and, because of the restricted nature of the experiment, a single drag coefficient curve results.

A procedure common to many studies of oscillatory motion and to some studies of unidirectional acceleration is to assume that the drag obeys the relationship

$$D = C_D \tfrac{1}{2} \rho V^2 \text{Area} + C_M m \dot{V} + C_H B(t) \qquad (7)$$

The assumption then usually is that C_D is the steady drag coefficient based on the instantaneous Reynolds number. This allows C_M and C_H to be inferred from measurements of the actual drag force. Alternatively, C_H might be assumed to be zero, and C_D and C_M evaluated as functions of a dimensionless acceleration or period pa-

rameter. In general, the applicability of the results is limited to the specific motion studied. Examples from the literature will serve to make this more clear.

1. Unidirectional Acceleration.

Impulsive start. Perhaps the most informative experiment is that of finding the drag on an impulsively started object. Recently, Dennis and Walker[26] have integrated the Navier-Stokes equations numerically over a wide Reynolds number range for impulsively started spheres. Beyond a Reynolds number of 100, their solutions are not of as fundamental interest because the flow is assumed to be axisymmetric while, as we have seen, in reality it is not. This forced axial symmetry prevents the shedding of vortices at Reynolds numbers as large as 1000, although, surprisingly, it has very little effect on drag coefficients calculated (e. g. Rimon and Cheng[24]). Dennis and Walker's nonsteady drag results may, therefore, be in error above 100 because of the forced axial symmetry, but certainly should be correct below 100. It is possible then to compare the unsteady part of the drag that would be predicted by the history term derived for Stokes flow, to see if the form of the history term is the same above the Stokes regime. Evaluating the third term in (3) for a sphere started impulsively at $t = o$, that is,

$$\dot{V}(t) = V\ \delta(o)$$

we get

$$B(t) = 6r^2\sqrt{\pi\rho\mu}\ V/\sqrt{t}$$

Using the same non-dimensionalization as Dennis and Walker, in order

to compare this to their numerical work, namely

$$t^* = V t / r$$

and defining a drag coefficient in the usual way, we get

$$C_D = C_{D_\infty} + (9.58/\sqrt{Re_d})/\sqrt{t^*} \qquad (8)$$

Note that contrary to the statement in ref. (35), the Basset part of the drag coefficient as derived here is not dependent on fluid density in any different manner than the steady drag.

Equation (8), as well as the numerical solution of Dennis and Walker, is shown in figure 3. It can be seen that the Basset term greatly overestimates the drag due to the impulsive start at Reynolds numbers of 20 and 100. This was not an expected result because the corresponding Stokes term for the steady drag underestimates the drag at Reynolds numbers of 20 and 100. Also, it is important to note that the time dependence of the numerical solution is not the same as that of the Basset term. For $t^* > 0.5$, the calculated drag coefficient is fitted accurately by the expression:

$$C_D = 2.69 + 0.9/t^*$$

That is, the numerically calculated drag decays as $1/t^*$, not as $1/\sqrt{t^*}$. Thus, this result supports our earlier statement that the Basset term must be changed by more than a constant at higher Reynolds numbers, i.e., a change in its form is required.

Constant acceleration. Sarpkaya and Garrison[36] have studied the drag for constant acceleration flow past cylinders at large Reynolds

numbers (the smallest Re when the cylinder had travelled one diameter was 23, 000). Acceleration varied between 1/6 and 2/3 g. They found that the drag, when non-dimensionalized by $\rho a \pi d^2/4$, was a function only of dimensionless position x/d (or equivalently dimensionless acceleration $V^2/2ad$). Using inviscid flow theory and motion picture studies of the vortex strengths, the authors break the drag up into C_D and C_M components. They show that C_D builds up to its steady value with an overshoot at $x/d = 2.5$, which is well before the position where the first vortex is shed[38]. However, their method of dividing the drag up into two parts is certainly suspect. An interesting comparison with the wake length studies of Honji and Taneda[38] is that of Tatsuno and Taneda[39] who show how strikingly different decelerating flow is from accelerating flow for cylinders.

Hamilton and Lindell[15] have done a meaningful experiment involving the concept of the added mass coefficient at moderate Reynolds number. The experiment involves moving a sphere at a steady Reynolds number, then accelerating the sphere and measuring the forces at the instant the acceleration begins. If the drag is represented as in equation (8) where $f(t)$ is an integral involving the history of the acceleration, the contribution from that integral will be zero at the instant the acceleration begins and the drag can depend only on the steady Reynolds number and the initial acceleration. Hamilton and Lindell's measurements with Reynolds number varying from 3, 300 to 35, 000 and with accelerations up to 0. 5 g show an added mass coefficient of 1/2 within 2 per cent in all experiments. This result is also

true, of course, when the initial Reynolds number is zero, and this has been verified by Roos and Willmarth[13].

These experiments form the basis of a logical division of sphere drag into component parts. The division is logical but arbitrary. The drag can be represented as in equation (8) with C_D taken as the steady value and C_M taken as 1/2. Then measurements in unsteady flows where the acceleration has a time history can be interpreted as measurements of the value of the history term. While this view does not increase our knowledge of unsteady drag, it does clarify some drag measurements, and the drag forces do reduce to the known values in the cases of steady flow and at the instant acceleration begins from any steady velocity.

Monotonic acceleration. Examples of drag measurements on monotonically accelerating spheres are the works of Ingebo[40] and Rudinger[10]. In these studies, the spheres are injected with zero velocity into a moving gas. The particle therefore starts with a large Reynolds number and a large deceleration (relative to the gas) and approaches a low Reynolds number and a low deceleration as it reaches the gas speed. Large deviations from the steady drag have been reported by both authors.

Ingebo, measuring particle accelerations (decelerations with respect to the gas) as large as 60,000 ft/sec^2, found that the drag was always less than the steady value and the largest deviation occurred at the largest Reynolds number. Only a small part of the drag change can be explained on the basis of an added mass concept, and this leads one to question whether or not the dimensionless accelerations are in-

deed large. Tatsuno and Taneda[39], in looking at the wakes of cylinders steadily decelerated from Re = 36.5 to rest, found that the wake adjusted in a quasi-steady manner for $ad^3/\nu^2 = .5$ and deviated only slightly from quasi-steady behavior for $ad^3/\nu^2 = 8.4$. Taking a typical measurement from Ingebo, that of a 40-micron particle in air, at an acceleration of 9,600 ft/sec^2 and a Reynolds number of 37, the value of ad^3/ν^2 is only 0.8. Therefore, the cylinder data suggest that although the actual accelerations are very large, the dimensionless accelerations used by Ingebo are small enough that the flow probably is quasi-steady. The explanation for the low drag coefficients may be in inaccuracies of the data which depend on the differentiation of only three position - velocity measurements, which were themselves only accurate to within 10 per cent. However, the correlation of the results by a single curve is unexpected; even if there is an acceleration effect, the acceleration parameter should be important also.

Rudinger, on the other hand, in indirect measurements made in shock tubes, finds that the drag coefficients calculated are larger than the standard value by a factor of 25 at Re = 10 and approach the standard value at Re = 300. No acceleration data are given, so it is not possible to determine whether or not the flow should be quasi-steady. Rudinger attempts to explain these results on the basis of perturbations to the particle paths and the effects thereof due to the nonlinearity of the drag law. However, as the nonlinearity is strongest at the largest Reynolds number, one might expect the largest deviation there, whereas it was actually smallest there. Some problems are probably connected with the indirectness of the measurements and

the need to differentiate experimental data, but it is difficult to explain away changes that are as large as a factor of 25. The explanation of Rudinger's data is, in this author's mind, still to be found.

Direct measurements of sphere drag in accelerating flows have been made by Roos and Willmarth[13]. During the initial stages of constant acceleration, the drag is that predicted by the added mass concept; but for spheres rapidly accelerated to constant velocity, the drag could overshoot the standard value by as much as 30 per cent.

2. Oscillatory Acceleration

Purely oscillatory motion. Keulegan and Carpenter[41], in a study of purely oscillatory flow past cylinders and plates, assumed a drag relationship as in equation (8) with $C_H = 0$ and calculated C_D and C_M from their force measurements. They found that these coefficients depended on the amplitude to diameter ratio, but were largely independent of the maximum Reynolds number developed. (This is not entirely unexpected as the Reynolds numbers $U_M d/\nu$ ranged between 4200 and 29,300, a range which is not greatly Reynolds number sensitive.) Large changes from quasi-steady values were found when $A/d = 2.5$, about the distance required to shed one vortex.

Odar and Hamilton[42] have investigated purely oscillatory motion past spheres with instantaneous Reynolds numbers always below 62: they found that the drag could be well predicted by equation (8) when C_D was taken to be the steady drag coefficient and C_M and C_H were functions of the instantaneous values of the parameter V^2/ad. However, application of their results to a non-oscillatory motion, e.g. the impulsively started sphere of Dennis and Walker, does not

predict the drag well. It seems clear that their results are limited to oscillatory motion at low Reynolds number.

Oscillatory motion with a mean flow. Measurements have been made of the terminal velocities of spheres in a vertically oscillating liquid. Data given by Baird, Senior and Thompson[16] and by Tunstall and Houghton[17] show changes in the mean drag by as much as a factor of 2 from the steady drag. Neither group recognized the dimensionless groups upon which the data could depend, and hence were unable to correlate their results. Baird, et al. recognized that the phenomenon was probably connected with vortex shedding, although they did not have the data to prove this. Tunstall and Houghton disbelieved the vortex shedding hypothesis and attempted to explain their data on the basis of a quasi-steady model, but they were not successful.

A problem closely related to this one is that of a cylinder undergoing transverse oscillations in a uniform freestream. In general, two situations have been considered; that of self-excited transverse oscillations of spring-mounted cylinders and that of forced transverse oscillations. The literature is fairly extensive on this subject in view of its application to self-excited motion of buildings and other structures. A comprehensive paper on the effects of vortex shedding on spring-mounted cylinders is that by Toebes[43]. Among the conclusions reached are the following: the strength and period of vortices vary randomly and only an average Strouhal number may be defined for $Re > 20,000$; cylinder oscillation leads to increased axial flow correlation; when the cylinder oscillation is at or near the natural shedding

frequency, the vortex strengths can be increased and the shedding frequency can shift to one near the frequency of the oscillation; the frequency of oscillation may also be affected if the oscillation frequency is at a multiple or submultiple of the natural frequency. The latter two results were also noted in an excellent paper by Bishop and Hassan[44] on the problem of forced transverse cylinder oscillations. They also measured large changes in the mean drag as the driving frequency was changed. The frequency of largest change was found to be always less than the Strouhal frequency, but approached the Strouhal frequency as the amplitude of the motion approached zero. No maximum in the response was found for amplitudes greater than one cylinder diameter. The range of synchronization of shedding with the forced oscillation was found to be approximately ± 20 per cent. This agrees with Koopman[45], who found these values to be somewhat amplitude- and Reynolds number-dependent.

Some concluding remarks about the drag of bluff bodies in unsteady flows are appropriate.

1. A self-consistant expression for the drag is of the form

$$D = C_D \tfrac{1}{2} \rho V^2 \text{Area} + C_M m \dot{V} + C_H \int_{-\infty}^{t} f(\dot{V}(\tau), \tau, t)\, d\tau \qquad (9)$$

where C_D is the steady drag coefficient and C_M is the coefficient measurable at the initial instant of acceleration, e.g., $C_M = \frac{1}{2}$ for a sphere or 1 for a cylinder.

2. In unsteady flows, the drag may differ considerably from

the steady value, particularly when the time scale involved is near the time required for vortex shedding. These changes may be interpreted as a measure of the third term in equation (9).

3. The function $f(\dot{V}(\tau), \tau, t)$ in equation (9) is unknown outside the Stokes regime. The probability of determining this function for Reynolds numbers above the Stokes regime is very small. In addition, the above data show unambiguously that $f(\dot{V}(\tau), \tau, t)$ is <u>not</u> the same function for high Reynolds numbers as for low Reynolds numbers.

III. EXPERIMENTAL

Before entering into a discussion of the apparatus and procedure used to measure the forces on a sphere in an oscillating liquid it is well to discuss the possible methods and their advantages and disadvantages. There are three possibilities to consider and each of these is pictured in figure 4. The first is that a rigidly mounted sphere shall be held in a fluid which is flowing with a mean velocity and a superimposed fluctuation. The second is that a sphere is fixed to an oscillating support and is in a fluid which is in uniform flow. The third possibility is that spheres are allowed to fall through a vertically oscillating liquid. The first two methods offer the advantage that instantaneous drag measurements may be made throughout the oscillation cycle. They both have the obvious disadvantage that the sphere must be supported and it is difficult to determine the effect of the support. Another distinct disadvantage is the inherent presence of free-stream turbulence in cases where the liquid is flowing. As we have seen in chapter II, freestream turbulence can have a pronounced effect on sphere drag. A further reason for making drag measurements of a falling sphere is that the sphere is free to respond to the fluid oscillations, as it is in many applications regarding two-phase flows.

In view of these considerations it was decided to make measurements of the mean drag in a falling sphere experiment. The apparatus is described in detail in the following section.

To aid in understanding the drag measurements, flow visualization studies were also carried out. These were done in a water tunnel for two main reasons. First, it is much easier to film the sphere close up if it is motionless. Second, the need to supply dye to the wake could easily be satisfied by bringing the dye in through the sphere support. Rather than oscillate the sphere and camera together, a simpler technique of causing the liquid to oscillate was employed. The flow visualization apparatus and procedure is also described in detail in the following section.

A natural question arises regarding the equivalence of these three experiments in terms of the flow fields and the drag forces in each. In fact, for a rigidly supported sphere the flow field is independent of whether the fluid or the sphere oscillates. The drag force differs only by the force due to the oscillating pressure gradient needed to support the fluid oscillation in the first case, hence the mean forces are the same for cases one and two. In the falling sphere experiment, when the sphere to fluid density ratio approaches infinity, ($\rho_s/\rho \to \infty$), the situation is equivalent to that of a rigidly supported sphere, apart from a Galilean transformation. Hence, the mean drag is the same in experiments one, two and three when the limit of infinite density ratio is approached for experiment three. Proof of these statements is given in Appendix B.

A. Apparatus

Drag Measurement

The experimental apparatus, shown in figure 5 and schematically in figure 6, consisted of a test section, an electrodynamic shaker, a means of introducing and retrieving spheres, and a timing mechanism to determine average sphere velocity.

The test section was a 3 inch I. D. by 4 foot long flared end glass pipe (Corning Glass Co.) clamped at each end to $\frac{1}{2}$ inch thick x 8 inch diameter aluminum discs and sealed with teflon gaskets. The discs were bolted together with four $\frac{1}{2}$ inch diameter steel rods. These rods were stressed, putting an added compression load on the pipe and insuring that tensile forces would not be taken by the glass. The upper aluminum disc was fitted with a $\frac{1}{2}$ inch standpipe leading to two quick-opening ball valves. The inner face of the upper disc was machined with a conical indentation the same diameter as the glass pipe to facilitate the removal of all air from the system when it was filled with liquid. The lower aluminum disc was bolted to the table of the electrodynamic shaker.

The shaker used in these experiments was a Ling, model A-175. This unit has a feedback control loop and is capable of producing motions corresponding to input signals from a signal generator. Only sinusoidal motions were generated in these experiments. The frequency range of the shaker is 5 to 4000 Hz. At low frequencies the table is limited to one inch peak-to-peak

displacement and at high frequencies to 1500 lbs. of force. In this case, the weight of the table and the apparatus is 75 lbs., limiting the acceleration to 20 g's above 20 Hz. An Endevco model 2242 accelerometer mounted on the shaker table monitors the acceleration of the apparatus and is included in the shaker feedback loop. The frequency of the oscillation is measured with a Hewlett-Packard model 521 DR electronic counter. In the experiments reported here frequencies ranged from 20 to 200 Hz and acceleration levels were limited to 10 g's.

The drop mechanism consisted of two valves connected to a $\frac{1}{2}$ inch diameter pipe, the inside of which was tapped to receive interchangeable brass tubes. Spheres were introduced to the test section through the brass tubes and the system could be kept closed at all times through the use of the two valves. Preliminary tests had shown that spheres dropped from a pair of tweezers did not tend to fall vertically downward but moved at an angle in a direction perpendicular to the line of the tweezers when the terminal Reynolds number was above 200. This led us to believe, and further tests showed, that a slight amount of initial rotation caused the ball to fall many diameters at what appeared to be a fixed angle before falling in a helical or zig-zag pattern with a mean motion that was vertical. This phenomena has been reported by Viets and Lee[54]. The helical or zig-zag motion of spheres is, of course, well reported in the literature[8, 47, 48, 54, 55]. In a tube of radius $1\frac{1}{2}$ inches, this meant

initial rotation could cause the sphere to move to the wall, where it would either fall stably against the wall or fall bouncing off the wall, on each bounce gaining enough rotation to force it back to the wall again. An electromagnetic drop mechanism had been used successfully by McLaughlin[46] in dropping steel spheres. This technique was not applied to the present experiment for three reasons: the complexity of the device which would have to be installed in the tube, the uncertainty of its success in the oscillating flow, and the restriction of using only magnetic spheres, as tests over a wide range of densities were desired. Baird, et al.[16] had reported dropping balls through a 5/8 inch diameter tube and had not reported any difficulty. In the present experiments the spheres entered the test section through tubes of approximately 1.2 ball diameters. Between 10% and 50% of the balls dropped in this manner fell straight enough to remain in a one inch diameter region in the center of the 3 inch diameter test section.

The retrieval mechanism was particularly simple. A $3\frac{1}{2}$ inch deep plexiglass insert was installed at the bottom of the test section. The insert had a conical depression machined in the top and a hole through the center. A 1/4 inch ID by 3 inch long brass bucket placed in the hole would catch the spheres and could be retrieved through the top of the apparatus when filled.

The timing mechanism, as shown in figure 6, comprised two light beams falling on two photocells connected to an electronic timing circuit. As noted previously, spheres falling at a Reynolds

number above 200 fall in helical or zig-zag patterns, the amplitudes of which are functions of the density ratio and Reynolds number. For this reason and because of the initial lateral motion of the sphere it was not possible to have the sphere block the entire light beam. Rather, a broad beam of small thickness ($1\frac{1}{2}$ inch by 1/16 inch) had to be used. It was then necessary to detect a small change in the light intensity when the sphere passed through the beam. Surprisingly, the thermal inertia of filaments is insufficient to prevent fluctuation in intensity the same order as this signal if alternating current is used. The light sources used were simply commercial flash-lights powered by 9 v batteries through rheostats so as to make the intensity adjustable. The light was passed through two $1\frac{1}{2}$ inch by 1/16 inch slits eight inches apart to produce a thin collinated beam. The beam, in passing through the liquid, was focused by the curvature of the water-glass, glass-air interfaces onto the 1/4 inch diameter face of the photocell. In preliminary experiments, with the two light beams parallel to each other, scatter in the terminal velocity measurements was the order of 10%. As the interest was in measurements of changes in terminal velocity, this was unacceptable scatter. The explanation for the scatter was that the initial motion of the sphere could cause it to move near the wall where it would have significantly higher drag. The solution to the problem was to put the light beams perpendicular to each other. Thus a time interval would be measured only for

spheres moving near the center of the test section, a sphere near the wall being able only to pass through one of the light beams.

The timing circuit, shown in figure 7, consisted of an amplifier and a monostable multivibrator. The signal from the photocell, resembling a 1/4 sine wave, was insufficient in magnitude and rise time ($\sim \frac{1}{100}$ sec) to run an interval timer. So it was amplified and fed into the monostable multivibrator. Adjustment of the 100-150 K variable resistor ensured that this signal, but not the noise, would trigger the multivibrator. The multivibrator in turn put out a 4.5 volt square wave with a rise time less than a microsecond. This pulse was sufficient to trigger a Hewlett-Packard model 5262-A time interval unit. Both photocells were connected to the same electronics to ensure that any time lag in the circuit would be the same for both and would not affect the measurement of the time inverval between the two beams.

The spheres used in these experiments were Hardford-Universal grade 200 type 440-C stainless steel, grade 200 type 2017 aluminum, tungsten Carbide and teflon. The sphericity (permissible difference between largest and smallest diameter) is given as .0002". Diameters ranged from 3/32 inch to 3/16 inch. Test fluids used were distilled water and mixtures of glycerin and water. For pure water, viscosities and densities were taken from ref. 56. For the water-glycerin mixtures viscosities were measured with an HV303 Hoeppler precision viscosimeter and densities were taken from ref. 56.

Visualization

Visualization studies were performed in an 18 inch x 20 foot free surface water channel with approximately an 18 inch water depth. Water entered the channel through a contracting nozzle with three sets of honeycombs as flow straighteners. A schematic is shown in figure 8. Uniform flows were created at a velocity of approximately 1/20 foot per second or a Reynolds number based on channel width of almost 10,000. Uniform flow with a superimposed oscillation could be obtained by producing a uniform flow, then throttling the valve on the return line which immediately decreased the flow rate. The excess of energy of the fluid in the channel then produced a primary shallow water surge wave in the channel. The effect of the surge wave was to produce a sinusoidal variation of the velocity near the geometric center of the channel. A similar technique had been used previously[41] to produce a pure sinusoidal flow, (i. e., no mean flow) and the resulting velocities have been analyzed extensively there. The surges produced in these experiments were of small magnitude, the largest having a peak of approximately 1/8 inch.

The model was a commercially available one-inch diameter plexiglass sphere with an interior cavity. The sphere was supported in the channel on a 25/1000 inch diameter stainless steel tube which entered through the rear stagnation point into the cavity. Four 25/1000 diameter holes were drilled from points on the sphere, calculated to be within the separated portion of the wake, into the

cavity. A potassium permanganate solution could then be injected through the tube into the cavity and out the four holes. This system insured an even distribution of dye to the four outlets. It is important that the support enter the sphere through the rear stagnation point. Goldstein[57] notes that this must be due to ensure correct drag measurements in wind tunnels and the reason was clearly seen in preliminary experiments. When the sphere is supported from the side (i. e., at the 90^{o} point in the flow) and the Reynolds number is such that the separation on an unsupported sphere would be greater than 90^{o} (more toward the rear of the sphere) the actual separation adjusts near the support so that it is in front of the support. This causes a significant change in the wake structure.

Motion pictures of the flow were made with a GAF ST110 8 mm movie camera. The frame time was calibrated by filming a stop watch. Fluid velocities were measured by introducing dye streaks into the free stream and differentiating distance-time results from analysis of the motion pictures. The period of the oscillation was measured independently by timing the rise and fall of the water level at the end of the tunnel. This could be done with some accuracy with a stop watch, as the periods were the order of 10 seconds.

B. Procedure

To determine the average velocity of a falling sphere, time elapsed as the spheres fell between the two light beams, described earlier, was measured and the average speed taken as the ratio of length between the beams and the travel time. This very simple measurement is complicated by the fact that for Reynolds numbers above 300, spheres do not fall in a straight line, but actually in a helical and/or a zigzag pattern, e. g., refs. 47 and 48. Consequently, the velocity as determined above is not the true velocity but the vertical component. Fortunately, this complication is not serious in the present work for two reasons.

First, in this experiment we are most interested in the ratio of the velocity in oscillating flow that that in steady flow. So long as the nature of the flow is unchanged, e. g. if the sphere still falls in a spiral in an oscillatory as well as a non-oscillatory flow, then the ratio of the vertical components of velocity will be meaningful. Visual observation of sphere trajectories indicates that for the conditions considered here, no changes in gross motion occurred when the tube was oscillated.

Second, these visual observations showed that the wave-length of the spiral or zigzag trajectories were of order of 8 - 12 inches or greater and had an amplitude less than one inch for the sphere trajectories used in making the drag calculations. Hence, the difference between vertical velocity component and true velocity magnitudes is less than 3 per cent for the trajectories studied here.

As a critical check on this procedure, steady state drag measurements were made in the Reynolds number range of interest. These results are shown in figure 9. On the expanded scale shown, the data appears to agree well with that of references 49-53 which are usually taken as the "standard drag curve"[58]. Also in agreement with this data but not shown is that of Roos and Willmarth[13]. The agreement with Roos and Willmarth data is significant as this data is obtained from tow tank measurements where the sphere is constrained to move in a straight line.

Because this experiment was designed to measure differences in terminal velocities, the accurate measurement of the velocities was particularly important. There was virtually no error in the timing between triggering due to the electronic means used. However, because of non-uniformities in the light beams, triggering could occur at different positions within the beams. For 1/16 inch thick beams placed 6 inches apart the maximum expected variation in velocities would be $\pm \frac{1/16}{6}$ or $\pm 1\%$. In fact, the scatter in the measured velocities was between $\pm \frac{1}{2}\%$ and $\pm 1\%$. To improve somewhat on this, at least ten measurements in still fluid and five in the oscillating fluid were taken so that the effects of the trajectories and the irregularities in triggering could be averaged.

In order to assure that there was no interference from the preceding sphere, about 10-15 seconds gap was left between releases. This would correspond to each sphere being roughly 2000 diameters behind the preceding one. In view of Torobin and

Gauvin's[4] measurements of the effects of free stream turbulence on sphere drag it is important that sufficient time be left between spheres so that the vortex wake left by the first sphere has time to dissipate. No significant changes were noticed in measurements taken with larger time intervals or between the first and subsequent measurements. In fact, as we will show later, disturbances at the vortex shedding frequency have a large effect on the drag, so that the drag of a sphere falling in the wake of an identical sphere could be greatly affected by that wake.

It was necessary to determine that the spheres had reached terminal velocity before measurements of their average velocities were made. Measurements of average velocity with an initial length of 25 and of 50 diameters showed no difference between the two. These results and previous work reported in the literature[48] show that, for the Reynolds number and density ratio covered, 25 diameters is sufficient for terminal velocity to be reached. In the experiments performed the sphere was allowed to fall at least 40 diameters before timing began. The results of figure 9 substantiate the conclusion that terminal velocity has been reached in all cases.

IV. ANALYSIS

The purpose of the experiment is to compare the terminal velocities of spheres in two situations -- one, the sphere falling through a quiescent liquid and two, the sphere falling through a liquid which is oscillating in the vertical direction. In each case a balance of the forces on the sphere implies that

$$m_s \frac{dU}{dt} = m_s g - m(g - \dot{V}) - D \tag{10}$$

where the terms on the right hand side represent, respectively the gravitational force, the force due to the pressure gradient in the fluid, and the fluid mechanical drag. Reference to Appendix B will explain the inclusion of the $\dot{V}$ term in the pressure gradient force with no qualifying assumptions. As we have shown in Chapter II the drag, D, in general depends on the relative velocity, the relative acceleration and the history of the relative acceleration between the sphere and the fluid. Independent of the form this takes, we see that when the sphere has reached a mean terminal velocity, in all cases

$$\bar{D} = (m_s - m) g$$

In the quiescent liquid $\bar{D}$ is the usual steady drag. Hence

$$(m_s - m) g = C_{D_o} \tfrac{1}{2} \rho U_o^2 \pi r^2 \tag{11}$$

In the oscillating flow we may define a force coefficient to be the mean drag normalized with $\frac{1}{2} \rho \bar{U}^2 \pi r^2$, in which case

$$(m_s - m) g = C_{\bar{D}} \frac{1}{2} \rho \bar{U}^2 \pi r^2 \tag{12}$$

Or, we may use the approach suggested in Chapter II, that the drag be divided into the steady drag, the added mass drag and a history drag. In this case

$$(m_s - m) g = (C_{D_o} + C_H) \frac{1}{2} \rho \overline{(U-V)^2} \pi r^2 \tag{13}$$

where

$$C_H \equiv B(t) / \frac{1}{2} \rho \overline{(U-V)^2} \pi r^2$$

because the added mass term has averaged to zero.

Comparing equations (11) and (12) we see that

$$C_{\bar{D}} / C_{D_o} = (U_o / \bar{U})^2 \tag{14}$$

and, therefore, while the mean drag is always $(m_s - m) g$ the mean drag coefficient increases if the terminal velocity decreases. If the changes in terminal velocity are small, then equation (14) becomes

$$\Delta C_D / C_{D_o} = -2 \Delta \bar{U} / \bar{U} \tag{15}$$

If we consider only velocity fluctuations small enough that

$$\overline{(U-V)^2} = \bar{U}^2$$

then dividing equation (13) by equation (11) we get

$$(C_{D_o} + C_{\bar{H}})/C_{D_o} = (U_o/\bar{U})^2 \qquad (16)$$

Comparing equation (16) and (14) we see that the change in the coefficient of the mean drag is just the coefficient of the mean history term.

A. Analysis of the Relative Motion

In addition to relating terminal velocity measurements to force coefficients, equation (10) can be used to analyze the relative motion between the sphere and the fluid under certain conditions. Breaking the drag up into three terms, we have:

$$m_s \frac{dU}{dt} = m_s g - m(g-\dot{V}) - C_D \tfrac{1}{2} \rho \pi r^2 (U-V)|U-V| - C_M m(\dot{U}-\dot{V}) - B(t) \qquad (17)$$

In this analysis of the relative motion we will take a position equivalent to that described in equation (12) when the fluctuations are small. Assume that C_D is defined such that all the mean drag is included in it i.e., $\overline{B(t)} = 0$.

Then the assumptions to be made are the following:

1. B(t) is small.
2. $C_M = \frac{1}{2}$.
3. the terminal velocity of the sphere has a mean value $\overline{U}$ and a fluctuating part U'.
4. the fluid undergoes oscillations such that the fluid velocity is $\omega A \cos \omega t$.
5. $\overline{U} >> U'$ and $\overline{U} >> \omega A$.

Equation (17) can then be rewritten

$$(m_s + 1/2\, m) \frac{dV_{rel}}{dt} = (m_s - m)(g + \omega^2 A \sin \omega t) - 3/4\, C_D m V_{rel}^2 / d \qquad (18)$$

where V_{rel} is the velocity of the fluid relative to the sphere. If we let $V_{rel} = \overline{V}_{rel} + V'_{rel}(t)$ and break equation (18) up into its mean and fluctuating parts we have

$$(m_s - m) g = 3/4\, C_D m \overline{V}_{rel}^2 \left\{ 1 + (V'_{rel}/\overline{V}_{rel})^2 \right\} / d \qquad (19)$$

and

$$(m_s + 1/2\, m) \frac{dV'_{rel}}{dt} = (m_s - m)\, \omega^2 A \sin \omega t$$

$$- 3/4\, (C_D/d)\, m \overline{V}_{rel}^2 \left\{ 2V'_{rel}/\overline{V}_{rel} + (V'_{rel}/\overline{V}_{rel})^2 - \overline{(V'_{rel}/\overline{V}_{rel})^2} \right\} \qquad (20)$$

If we now assume that $V'_{rel}/\overline{V}_{rel}$ is small compared with unity it is apparent that C_D is equivalent to $C_{\overline{D}}$ defined in equation (12) and that equation (20) is integrable. Integration

of (20) results in

$$V'_{rel} = \frac{(m_s - m)\,\omega^2 A}{\left\{ (3/2\, m\, C_D \overline{V}_{rel}/d)^2 + \omega^2 (m_s + 1/2\, m)^2 \right\}^{1/2}} \sin(\omega t - \phi)$$

where

$$\phi = \cos^{-1}\left[\frac{3/2\, m\, C_D \overline{V}_{rel}/d}{\left\{ (3/2\, m\, C_D \overline{V}_{rel}/d)^2 + \omega^2 (m_s + 1/2\, m)^2 \right\}^{1/2}} \right]$$

Then A_p, the amplitude of the motion relative to the sphere is given by

$$A_p/A = \frac{(m_s - m)}{\left\{ (m_s + 1/2\, m) + (3/2\, m\, C_D \overline{V}_{rel}/\omega d)^2 \right\}^{1/2}} \qquad (21)$$

The term $3/2\, m\, C_D \overline{V}_{rel}/\omega d$ is the effect of the change in the drag force due to the change in velocity. This, of course, involves a quasi-steady assumption about the fluctuating drag forces that we are not prepared to make. The interest in equation (21) is when these fluctuating forces are small. That is, if

$$1/2\, [(m_s + 1/2\, m)/(m_s - m)] (\omega \overline{V}_{rel}/g) \gg 1 \qquad (22)$$

then $$A_p/A = (m_s - m) / (m_s + 1/2\, m)$$

or $$A_p/A = (\rho_s/\rho - 1)(\rho_s/\rho + 1/2) \qquad (23)$$

This relationship, while based on assumptions that are not entirely justifiable, at least agrees with our intuition of the behavior at the density limits. We expect that when $\rho_s/\rho = 1$, the particle follows the fluid motion identically and therefore the amplitude of the relative motion is zero. We also expect that when $\rho_s/\rho \to \infty$ the particle no longer responds to the fluid forces and the amplitude of the relative motion is then equal to the amplitude of the fluid motion. A more general proof of this last statement is given in Appendix II.

Equation (23) will be the basis for determining the dependence of the drag results on density ratio.

Equation (23) also provides a simple basis for calculating the effect on the drag coefficient expected from a quasi-steady drag model. For such a model

$$D = C_{D_o}\, 1/2\, \rho\, V_{rel}^2\, \pi r^2$$

or

$$D = C_{D_o}\, 1/2\, \rho\, (\bar{V}_{rel} + \omega A_p \sin \omega t)^2\, \pi r^2$$

Taking the mean value

$$\bar{D} = C_{D_o} \tfrac{1}{2} \rho \left[\bar{V}_{rel}^2 + \tfrac{1}{2} (\omega A_p)^2 \right]$$

and

$$C_{\bar{D}} = C_{D_o} \left[\bar{V}_{rel}^2 + \tfrac{1}{2} (\omega A_p)^2 \right] / \bar{V}_{rel}^2$$

or

$$\Delta C_D / C_{D_o} = \tfrac{1}{2} (\omega A_p / \bar{V}_{rel})^2 \qquad (24)$$

Equation (24) will be used to estimate the change in the coefficient of the mean drag caused by an oscillating fluid on the basis of a quasi-steady drag model.

B. Dimensional Analysis

Consider the mean terminal velocity of a sphere falling under the influence of gravity in a vertically oscillating liquid. The mean terminal velocity, $\bar{U}$, will be a function of seven variables, namely

$$\bar{U} = f_1 \{ d, \rho_s, \nu, \rho, f, A, g \} \qquad (25)$$

where the first six variables describe, in pairs, respectively, the sphere, the fluid, and the oscillation of the fluid. The last variable represents the gravitational force, the driving force for

the motion. However, representation of the data in terms of this set of variables would limit the application of the results to this particular situation -- a sphere falling under the influence of gravity. Consider the example discussed briefly in Chapter III of a sphere, rigidly supported in a tunnel. Appendix B shows that the mean drag is the same as that for this experiment in the limit of density ratio going to infinity. But in the tunnel experiment there is no equivalent of g, (other than the force required to move the fluid through the tunnel). A more appropriate variable than g is found through the application of equation (11) from which

$$g = \frac{C_{D_o}\{U_o d/\nu\} \cdot 1/2\, \rho U_o^2 \pi r^2}{4/3\, \pi r^3 \ (\rho_s - \rho)}$$

It is obvious that U_o, the terminal velocity in the absence of the fluid oscillation, may be used in place of g, resulting in

$$\bar{U} = f_2\{d, \rho_s, \nu, \rho, f, A, U_o\} \qquad (26)$$

We will show later that this representation applies to both types of experiment.

The application of dimensional analysis implies that there will be a unique relationship between (at maximum) five independent dimensionless groups formed from the eight variables. While any

five such groups will serve to represent the data, the choice of a physically pertinent set may represent it in a particularly simple fashion. The representation chosen in this work is

$$-\overline{\Delta U}/\bar{U} \triangleq (U_o - \bar{U})/\bar{U} = f_3\left\{Re, A/d, f/f_{ST}, \rho_s/\rho\right\} \quad (27)$$

This choice of dimensionless variables is a logical one. The drag should be a function of the mean Reynolds number, the ratio of the amplitude of the motion to the sphere diameter, and the sphere to fluid density ratio. Based on previous experiments reported in Chapter II it is clear that the time taken for a vortex to build and shed is a characteristic time for the system at least where vortex shedding occurs. In the oscillating liquid the flow will certainly be altered. But a reasonable frequency to use for the non-dimensionalization is the frequency at which vortices would be shed if the sphere were travelling at a steady velocity $\bar{U}$ and Reynolds number Re. At low Reynolds number where no shedding occurs a suitable dimensionless frequency would be fd^2/ν.

Ideally the object of the experiment would be to vary each of the parameters independently to determine the dependence of $\overline{\Delta U}/\bar{U}$ on each. A simple example will show, however, that this is very difficult to do in the present experiment. If the sphere terminal velocity is affected by the parameter A/d, then if A/d varies so does the mean Reynolds number Re and the natural shedding frequency f_{ST}. Moreover, the changes are not known until

the experiment is performed. Hence, keeping Re and f/f_{ST} fixed while varying A/d would require an iterative experimental procedure.

Quantities which are closely related to Re and f_{ST} when $\Delta\bar{U}/\bar{U}$ is small are Re_o, the oscillation free Reynolds number and f_{ST_o}, the natural vortex shedding frequency in the steady flow. It is possible to represent the data as

$$-\Delta\bar{U}/\bar{U} = f_4\left\{ Re_o, A/d, f/f_{ST_o}, \rho_s/\rho \right\} \qquad (28)$$

In the limit as $\Delta\bar{U}/\bar{U} \to 0$, $R_e \to Re_o$ and $f_{ST} \to f_{ST_o}$, so the function f_3 (eqn.27) approaches the function f_4. But as $\Delta\bar{U}/\bar{U}$ becomes large, a simple relationship in (27) necessarily becomes a more complicated one in (28) because the transformations from Re to Re_o and from f_{ST} to f_{ST_o} involve $\Delta\bar{U}/\bar{U}$ itself.

In the analysis of the relative motion presented in the previous chapter, it was found that the motion of the fluid relative to the sphere was a uniform flow with a superimposed oscillation of amplitude A_p. The results of Appendix B show that the flow field is independent of the actual acceleration of the fluid and depends only on the relative motion. Therefore if the analysis is correct, the results found in the oscillating flow must correspond to those found in a tunnel experiment with the same A_p/d and

$$-\Delta\bar{U}/\bar{U} = f_5\left\{ Re, f/f_{ST}, A_p/d \right\} \qquad (29)$$

That is, the effect of the density ratio is only through its affect on the magnitude of the relative motion. Independent of the analysis of the previous section it has been shown that the two experiments measure the same mean drag (Appendix B) if $\rho_s/\rho \to \infty$. Making use of equation (14) we have

$$C_{\bar{D}} / C_{D_o} = \left[1 - \Delta\bar{U}/\bar{U} \right]^2$$

and values of the drag for a sphere, rigidly mounted in a tunnel would be found from

$$C_{\bar{D}} = \lim_{\rho_s/\rho \to \infty} C_{D_o} \left[1 + f_3 \{ Re, A/d, f/f_{ST}, \rho_s/\rho \} \right]^2$$

V. RESULTS AND DISCUSSION

A. Drag Measurements

Measurements of the mean terminal velocities of spheres in a vertically oscillating fluid have been made in the Reynolds number range $.2 < Re < 3000$ for a variety of frequencies and amplitudes of oscillation. As we have shown, measurements of the terminal velocity are simply related to the values of the mean drag coefficient, eg., equation (14). The dimensionless frequency, fd/U, of the oscillations was of order unity in all cases. Therefore the flow could not be assumed *a priori* to be quasi-steady. The results of these measurements will be given for the Reynolds number ranges in which vortex shedding does and does not occur; in addition, flow visualization measurements made in the vortex shedding range will be presented.

Measurements in the Range $.2 < Re < 100$

The sphere wake in a steady flow is stable throughout this Reynolds number range. For the lowest Reynolds numbers used the steady drag is proportional to the velocity while at the highest it is more nearly proportional to the velocity to the three halves power. For a nonlinear drag law of power greater than one it is obvious that a quasi-steady fluctuation will increase the mean drag. This effect, of course, increases with increasing exponent in the drag relationship so the effect increases with increasing Reynolds number. In the experiments performed here, the

velocity fluctuations are such that negligible changes in the drag are predicted by the quasi-steady drag law. At low Reynolds numbers the fluctuations were large but the exponent is small, while at large Reynolds numbers the fluctuations were small. Table I shows the range of dimensionless frequency, velocity and amplitude covered. Oscillation amplitudes ranged up to 5 diameters at the lowest Reynolds number and up to .45 diameters at the highest Reynolds number. No appreciable change (>2%) in terminal velocity was found for any of these experiments. Although the frequencies were such that quasi-steady drag could not be assumed, no deviation in the mean drag was found that was inconsistant with quasi-steady drag. The fluctuating components could, of course, not be determined. The significance of these measurements is better appreciated when a comparison is made with the measurements taken in the range where vortex shedding occurs.

TABLE 1

Ranges of Variables Covered For Re <200

Re	$\frac{fd}{U}$	$\frac{\omega A}{U}$	$\frac{A}{d}$
100	.04-.5	.1	.45-.05
60	.13-.2	1.1-.5	1.4-.5
3	.2-1.2	1.2-.8	1.0-.13
.2	.5-1.5	30-10	5-.5

Measurements in the Range $600 < Re < 3000$

As we have described previously, in this Reynolds number range the sphere sheds discrete portions of the wake with apparent complete regularity for Reynolds numbers below 700 and with some irregularity for Reynolds numbers above 700. We have chosen, therefore, to investigate the effect of the oscillation on sphere drag through the parameters Re, A/d, ρ_s/ρ and f/f_{ST} as discussed in the section on dimensional analysis. Throughout this section we will assume that the Strouhal frequency f_{ST} is given by the extension of Goldburg and Florsheim's[31] result for $270 < Re < 700$, namely

$$f_{ST}\, d/U = 0.387\,(1 - 270/Re) \qquad (30)$$

The similiarity of this form with the well known results for circular cylinders suggests that(30) may be valid for larger Reynolds numbers and this equation will be applied to the whole Reynolds number range examined here.

Note that Appendix A lists sufficient information on the dimensional variables that all dimensional quantities may be reconstructed for all the experimental data.

The suitability of non-dimensionalizing with f_{ST} is demonstrated well by figure 10 which shows the effect of f/f_{ST} on the terminal velocity change $(-\Delta\bar{U}/\bar{U})$ for various values of Re, A/d and ρ_s/ρ. The oscillation appears to produce very small changes in terminal velocity for frequencies below

0.25 f_{ST} or above 3.5 f_{ST}. The response to the oscillation peaks near $f/f_{ST} = 1$, maintains a large amplitude out to $f/f_{ST} = 2$ and then decays rapidly as f/f_{ST} increases beyond 2. An important feature of the curves that relates to the choice of f_{ST} as a natural frequency is their similarity of shape. Changes in Re_o, A/d and ρ_s/ρ appear only to change the magnitude of the effect. Note that f_{ST} is the frequency, calculated from equation (30), at which vortices would be shed in a steady flow which had the mean velocity $\overline{U}$ and mean Reynolds number $Re = \overline{U}d/\nu$. In this figure, actual frequency values differ by approximately a factor of 3 between the upper and lower curves so the non-dimensionalization with f_{ST} is, in fact, significant.

All the data show a decrease in terminal velocity or an increase in mean drag coefficient as a result of the oscillation. Using equation (14) it may be seen that the 10% change in terminal velocity of the uppermost curve represents a 21% change in the mean drag coefficient with an amplitude of oscillation that is only 2% of the sphere diameter. A quasi-steady drag model predicts that the oscillation will produce a decrease in terminal velocity due to the quadratic drag law and the difference between $\overline{U}^2$ and $\overline{U^2}$. However, equation (24), which is the result of such a model, predicts only a 0.05% change in the mean drag coefficient. In fact, all quasi-steady predictions are so small as to make them indistinguishable from the horizontal axis and, as such, have not been plotted.

There is some experimental difficulty in performing experiments such as these, a constant amplitude over a wide range of frequencies. If the frequency changes by a factor of 7 (e.g., from .5 f_{ST} to 3.5 f_{ST}) then the peak acceleration level developed by the shaker changes by a factor of 50. For this reason subsequent data is shown over a smaller frequency range.

In figure 11 the effect of dimensionless frequency on terminal velocity is shown for $A/d = 0.02$ and different values of density ratio and Reynolds number. Again, the similarity of the curves is quite striking, particularly for $f/f_{ST} < 1$. A comparison of the lower and upper curves shows the effect of changing the Reynolds number in the undisturbed flow from 1750 to 2800. The effect under study clearly increases as Reynolds number is increased for all values of dimensionless frequency considered. Note also that the curve for $Re_o = 2050$ and $\rho_s/\rho = 14.0$ is approximately where it would be if density ratio had no effect between 7.83 and 14.0 and a linear interpolation in Reynolds number were made between the other two curves. The actual effect of density ratio is shown more explicitly in figure 15.

Again, in figure 12, the effect of f/f_{ST} on terminal velocity is shown for a somewhat smaller frequency range. The parameter which changes between the curves is the amplitude of oscillation to sphere diameter ratio. This ratio changes by a factor of 1.5 between the lower and middle curves and by a factor of 2 between

the lower and upper curves. It can be seen that for frequencies below about $0.7\ f_{ST}$, the percentage change in terminal velocity is approximately proportional to amplitude ratio but for frequencies above this value it is not. To see more clearly the effect of amplitude ratio it is convenient to consider sections through these curves, i.e., to consider the variation of $\Delta\bar{U}/\bar{U}$ with A/d at various constant values of f/f_{ST}. As was mentioned earlier, it was not practical experimentally to do experiments at constant f/f_{ST} and the curves shown in figure 13 are at constant values of f/f_{ST_o}. It can be seen that for small values of f/f_{ST_o}, the fractional change in terminal velocity is linear in A/d but for f/f_{ST_o} near unity the effect becomes nonlinear, actually increasing approximately as $(A/d)^{2/3}$.

That the effect is linear at $f/f_{ST_o} = 0.6$ for various Reynolds numbers is demonstrated in figure 14. The lower three curves show the effect of varying Re_o for a density ratio of 2.83 and show a monotonic increase of effect with increasing Reynolds number from $Re_o = 845$ to $Re_o = 2020$. The uppermost curve is at a Reynolds number intermediate to this range ($Re_o = 1750$) but is at a higher density ratio. So at least at this Reynolds number the effect is dependent on density ratio.

The linear dependence between $\Delta\bar{U}/\bar{U}$ and A/d as shown here is the basis of the choice of $\Delta\bar{U}/\bar{U}$ as independent variable. A more natural choice for independent variable might be $\Delta\bar{U}/\bar{U}_o$ which, for the changes shown here, will still very nearly be linear in

A/d. However, there is no possibility that $\Delta\bar{U}/\bar{U}_o$ can be proportional to A/d for A/d even as large as unity. Consider the data shown for $Re_o = 1410$ and $\rho_s/\rho = 2.83$ where $\Delta\bar{U}/\bar{U}$ is equal to A/d. An extension of this relationship to A/d = 1 would imply that the sphere would fall at one half the undisturbed terminal velocity. But if $\Delta\bar{U}/\bar{U}_o$ had been used it would imply that the sphere would be stopped by the oscillation--clearly an unreasonable suggestion. It is not unreasonable to suggest, however, than an infinite amplitude oscillation could stop the sphere, which is what is implied by having $\Delta\bar{U}/\bar{U}$ equal to A/d.

The linearity of the effect at $f/f_{ST_o} = 0.6$ allows a more detailed examination of the effects of density ratio and Reynolds number. The slopes of curves such as in figure 14 serve as indications of these effects. Each data point in figure 15 represents the slope of such a curve. From figure 15 it is clear that the effect of the oscillation increases as the Reynolds number increases from 650 to 3000. The effect of the oscillation is also seen to increase with increasing density ratio. The density ratios given in figure 15 are given as approximate values because in some cases glycerin-water mixtures were used to achieve appropriate Reynolds numbers. The actual values may be obtained from Appendix A. An important feature of the density ratio effect is that it appears to be converging as ρ_s/ρ increases. Reference to Appendix II will show that the results of this experiment will apply to drag changes on rigidly mounted spheres when $\rho_s/\rho \to \infty$.

The density effect seen in figure 15 supports the intuitive idea expressed in the analysis of the motion, presented earlier. The expectation was that light spheres would tend to follow the fluid motion more closely, hence would see less relative motion and hence would be affected less by the fluid oscillation. It appears to be reasonable then to apply the results of the previous analysis, namely that

$$A_p = [(\rho_s - \rho)/(\rho_s + 1/2\,\rho)]\,A$$

If the relative motion has sinusoidal fluctuations, the effect can depend only on the relative motion, the actual acceleration of the fluid having no effect on the mean drag (Appendix II).

The application of this analysis to figure 15 gives figure 16 in which $\Delta\bar{U}/\bar{U}$ is normalized by the calculated A_p/d rather than by A/d. Again, density ratios are shown as approximate values because of the slightly different fluids used. The actual values, as given in Appendix A, were used in calculating the ordinate. It can be seen in this figure that the effect of density can, within reasonable error bounds, be incorporated into its effect on the relative amplitude A_p.

Figure 16 also shows the effect of Reynolds number on the change in terminal velocity more clearly. The effect is seen to be approximately linear in Reynolds number and approaches zero as Reynolds number approaches zero.

So far, the analysis of the relative motion has only been applied at one dimensionless frequency, $f/f_{ST_o} = 0.6$. Figure 17 shows the results of an experiment designed to test the hypothesis over a range of frequencies. A comparison of the lower two curves will show that effect of a 50% change in amplitude when density ratio is held constant is readily measurable. The filled and unfilled triangular symbols show the effect of a 50% change in amplitude when the density ratio is adjusted so that the calculated value of A_p is unchanged. It is clear that the data is well represented by the variable A_p/d rather than by the two variables A/d and ρ_s/ρ .

It should be noted that no attempt was made to measure A_p. Measurement of A_p would have required high speed motion pictures recording both the motion of the sphere and the fluid so that the relative motion could be determined. But, as the amplitudes involved were at most 1/100 of an inch, even 10% accuracy would have required determination of the sphere position to within 1/1000 of an inch--an extremely difficult task.

The correlations seen in the previous figures can be combined, and this is done in figure 18. Because the results were shown to be linear in A_p/d and in the Re above Re = 200 these are included in the ordinate. The dashed line represents the curve $12.25\,(f/f_{ST})^2$.

Also shown in figure 18 are data of references (16) and (17) for which the Reynolds number is greater than 500. This

limitation was made because of the error inherent in the choice of the limiting Reynolds number in the correlations (200 in the Reynolds number effect and 270 in the vortex shedding frequency). The data of reference (16) is most significant because it extends the density ratio to values much closer to unity and the amplitudes used were as large as 13 sphere diameters. In spite of the low densities the motion relative to the sphere, as estimated by equation (23) is still as large as 1.5 sphere diameters. The implication is that the correlation is valid over a much larger density and amplitude range than those covered in the present experiment. The scatter in the data is slightly larger than that expected from experimental scatter alone and probably indicates that the exact dependence on dimensionless variables is more complicated than the one given here in equation (31) on page 57.

This correlation has shown that, for $f/f_{ST} < 0.7$ the change in terminal velocity is proportional to the product $(Re-200)\ A_p/d$. Data presented in figure 13 showed that near the Strouhal frequency the dependence on amplitude was more nearly like $(A/d)^{2/3}$. On this basis alone the peak data are shown in figure 19 as a function of $[(Re-200)\ A_p/d]^{2/3}$. These data are also tabulated in Appendix A. The deviation of the data points from this correlation is within experimental scatter.

The representation for the data then is

$$-\Delta\bar{U}/\bar{U} = (12.25/2800)(Re-200)(A/d)\left[(\rho_s-\rho)/(\rho_s+1/2\,\rho)\right](f/f_{ST})^2$$

$$0 < f/f_{ST} < 0.75 \qquad (31)$$

and

$$-\Delta\bar{U}/\bar{U} = 0.011\left\{(Re-200)(A/d)\left[(\rho_s-\rho)/(\rho_s+1/2\,\rho)\right]\right\}^{2/3}$$

$$f/f_{ST} = 1 \qquad (32)$$

In each case, coefficients of the mean drag are given by

$$\Delta C_D/C_{D_o} = (1-\Delta\bar{U}/\bar{U})^2 - 1 \qquad (33)$$

B. Flow Visualization

It is clear from the analogous case of oscillating cylinders that the mechanism for the change in sphere drag in an oscillating flow should be a change in the strength and possibly the frequency of vortex shedding. However, the related cylinder work is somewhat different as most investigations concern transverse oscillations rather than oscillations in the direction of the flow. No careful study has been made of the sphere wake in an oscillating flow. In the present visualization study the Reynolds number ranged from approximately 400 to 600. In this regime, according to Magarvey and Bishop[8] and Goldburg and Florsheim[31], the natural shedding of vortices takes the form of a double row of vortex rings. Unfortunately, because of the turbulence level in the free surface tunnel used in this experiment, we were unable to verify this fact in steady flow. The presence of free stream turbulence causes the vortex shedding to become irregular, both in form and in frequency. At irregular times a portion of the wake moves downstream but the structure of the shed portion of the wake does not appear to be well defined. Upon the superposition of a small amplitude oscillation, however, the shedding becomes regular in time and in form. In this Reynolds number range the shedding observed in the oscillating flow was always that of the procession of vortex loops, reported as a Class IV wake in the work of Margarvey and Bishop[8]. In fact the appearance of the wake is very similar to the example they show in plate V. This is somewhat surprising as they show Class IV

wakes in steady flow exist only to a Reynolds number of 410 and beyond this a double row of vortex rings is seen. An explanation of this apparent contradiction may possibly be found in Magarvey and Bishop[32] in which they show the wake of a droplet showing what appears to be vortex loops, and a picture of the same wake 10 seconds later which appears to show clearly the presence of vortex rings. It appears that the evolution of the vortex loops, once they are shed, is such as to make them resemble vortex rings connected by thin loops. So it may well be that even to much larger Reynolds number the shedding near the sphere resembles that of the vortex loop shedding.

When a sphere is falling under the influence of gravity the pattern of vortex shedding is (c.f. ref. (31)) one of the loops being shed from alternate sides of the sphere. The diameter about which this shedding occurs rotates with a circular frequency much smaller than the shedding frequency and this accounts for the helical pattern of the wake and the motion of the sphere. In the present study, while this alternate shedding from one side of the sphere and then the other occurred in all cases, the orientation of the diameter about which this happened was in all cases fixed in the vertical direction. This may have been caused by the slight density difference between the dye and the water or possibly by a slight asymmetry in the support.

Measurements were made of the position of the shed vortex loop as it was moved downstream. The actual position measured was a visual judgement of the centroid of the mass of dye ejected from

the wake. The first of these results is seen in figure 20 where the mean Reynolds number is 580, the frequency of the oscillation is 63% of the frequency at which vortex shedding would occur naturally in a steady flow at a Reynolds number of 580, and the amplitude of the oscillation is 42% of the sphere diameter. The solid line shows the velocity of the freestream relative to the sphere. The symbols and the dashed line through them represent the downstream position of the vortex in sphere diameters as measured from the center of the sphere. The time coordinate has been adjusted so that one more period of the oscillation is subtracted for each succeeding vortex. Coincidence of the results for several vortices implies that vortex shedding is occurring at the frequency of the oscillation, rather than at the natural frequency. As can be seen in figure 20 the vortex loop begins to move away from its position behind the sphere about the time the velocity is increasing through its mean value. At this large an amplitude of oscillation, a large portion of the wake is shed in each vortex loop, the loops are quite distinct and the measurement of the position is quite repeatable. When the amplitude is smaller, as it is in figures 21, 22, the measurement becomes more difficult as a less distinct loop is shed. However, the results shown for $f/f_{ST} = .85$ are similar to those for $f/f_{ST} = .63$. Vortex shedding occurs at the oscillation frequency rather than the natural frequency and again the vortex begins to move rapidly away from the sphere as the velocity increases through its mean value. However, the vortex has moved to about

1.7 diameters downstream as the velocity has increased to the mean whereas at $f/f_{ST} = .65$ the vortex is only about one diameter downstream before its velocity changes rapidly. For $f/f_{ST} = 1.33$ as shown in figure 22 the situation is much the same. Vortex shedding occurs at the imposed frequency and the vortex loop moves away from its position about 1 diameter downstream when the freestream velocity increases through its mean. A more valid comparison of these figures can be made when the time coordinate is non-dimensionalized as it is in figure 23 by $\overline{V}/d$. The coordinate in this case represents the position of a particle in the freestream moving at the average freestream velocity. In other words the slope of the x/d for the vortex approaches unity as its velocity approaches the freestream velocity. Here it can be seen that the downstream position is to some extent dependent on the dimensionless variables A/d and f/f_{ST} and the explanation is obvious. Large amplitude oscillations deplete more of the wake implying that as the wake builds up it will be closer to the sphere. Oscillations at large frequencies will also have the same effect. The results do show, however, that in the range from $f/f_{ST} = .65$ to $f/f_{ST} = 1.37$, vortex shedding occurs at the imposed frequency and no significant change in the phase angle of shedding occurs.

Observations of the separation position showed clearly that the separation position varied by up to 10^{o} as the freestream velocity varied. This raised the question--could oscillations produce similar effects on bodies for which the separation point is fixed? To de-

termine this, drag coefficients of $\frac{1}{4}$- inch diameter, 70 degree cones were measured at a Reynolds number of 4000 in the same manner as the sphere drag tests. The results of these tests show a 15.5% change in drag coefficient for a 4% amplitude to diameter ratio -- a change comparable to that found for spheres. The implication is that bodies with fixed separation points will also be sensitive to fluid oscillation.

C. Discussion

Data representing the drag on spheres in an oscillating flow has been presented which shows the drag is dependent on A/d, ρ_s/ρ, Re and f/f_{ST}. Several features of the drag and the visualization suggest strongly that a non-linear resonance with the sphere wake is responsible for the large changes in the mean drag at moderate Reynolds numbers. These include a maximum change in drag coefficient at the Strouhal frequency and the shedding of vortices at the imposed frequency of oscillation.

The most important feature of the representation of the present data was the choice of the mean speed $\overline{U}$ and the Strouhal frequency f_{ST} (based on the mean speed) as the variables upon which to base the non-dimensionalization. This choice was not obvious at the outset, as a comparison was being made between a steady flow with velocity U_o and vortex shedding frequency f_{ST_o} and an oscillating flow with mean velocity $\overline{U}$ and it seemed natural to describe the change in terminal velocity in terms of U_o and f_{ST_o}. Upon examination of the data, however, it became apparent that the peak response shifted to lower values of f/f_{ST_o} as A/d was increased and $\Delta\overline{U}/\overline{U}$ increased. This shift could be explained by the fact that as the mean velocity decreased the frequency of natural unsteadiness in the wake decreased. But this frequency is likely to be well represented by f_{ST} which is the vortex shedding frequency in a steady flow at speed $\overline{U}$ and Reynolds number $Re = \overline{U}d/\nu$.

Baird, et al.[16], in an experiment similar to the one here, recognized that the phenomena was connected with vortex shedding, but thought that the data could be represented solely in terms of A/d and fd/U. They ignored density and Reynolds number effects although these parameters did vary throughout the experiments. The nondimensionalization of frequency with U/d also ignores the change in Strouhal number with Reynolds number and would therefore show peak response at various dimensionless frequencies, depending on the Reynolds number.

The authors of reference 17, who performed a similar experiment, disbelieved the vortex shedding hypothesis and attempted to explain the data on the basis of an irrational multiple free parameter quasi-steady model, an attempt which failed. In addition, it has been shown here that the changes in terminal velocity are too large to be explained on the basis of any rational quasi-steady model.

A significant feature of the present work is that, although the amplitude range was small (up to 13% of the sphere diameter), the choice of correlating parameters was such as to enable correlation of the data of reference 16 where amplitudes were much larger. If the correlation of the present data had been made on the basis of $\Delta\bar{U}/U_o$ instead of $\Delta\bar{U}/\bar{U}$ and f/f_{ST_o} instead of of f/f_{ST} the data of reference 16 could not have been correlated.

The lower limit of Reynolds number at which the oscillation produces significant effect has been found from extrapolation of the data of figure 16 to be Re = 200. This Reynolds number limit is in agreement with that found by Zarin and Nicholls[12] for the effect of freestream turbulence on sphere drag. Reference 12 also reports an increase in the effect as Reynolds number increases, although the increase is not as linear as in the present work.

The interpretation of turbulence results in terms of the present work, however, is not easily done. Part of the motivation of this work was to understand turbulence measurements when the particle is much smaller then the turbulence scale, for in this case the particle would appear to be moving through regions of varying velocity in a very simplified picture. However, the frequency at which the velocity would vary would be given approximately by

$$f = V_{rel} / \lambda$$

where λ is the turbulence scale length, and the dimensionless frequency would be given by

$$f d / V_{rel} = d / \lambda$$

Hence, if the diameter is much smaller than the turbulence scale the dimensionless frequencies will be small. But if the dimensionless frequence is below about 0.1 (1/4 of the Strouhal number) the varying velocity should appear to be quasi-steady, and hence no effect of the type found here would be expected. Admitted-

ly, this is a very simplified view of turbulence and may not be valid. The prediction of quasi-steady behavior is not subject to verification, as work to date[4, 12, 20, 36] has been performed with turbulence scales the same order as the sphere diameter, where such a simple view of the flow cannot be taken.

An effect that might be expected, regardless of the order of the turbulence scale, is a diameter effect. The only report of such an effect is in ref. 12, and there an inverse diameter effect on drag increase is found only when the turbulence is generated by screens very close to the sphere. In this case, the distribution of the turbulent fluctuations may be more sharply peaked about a single frequency, and the situation might appear in closer analogy to the present experiment in which, over a wide range of frequencies, the drag change was proportional to A/d.

The measurements of ref. 4 of the effects of freestream turbulence were interpreted as indications that freestream turbulence caused turbulent reattachment of the laminar separation, even at as low a Reynolds number as 370. The observations here of a sphere in a steady but turbulent freestream show that the turbulence has a pronounced effect on the near wake, and it is suggested that at low Reynolds numbers this might account for the change in drag coefficient.

VI. CONCLUSIONS

The terminal velocities of spherical particles in a vertically oscillating fluid have been studied. The terminal velocities are directly related to the mean drag coefficient. The mean drag coefficient can be dramatically increased if the oscillation is at a frequency near the frequency at which vortices would be shed in a steady flow at the mean speed. Empirical correlations have been presented for the mean drag coefficient. From the frequency response of the terminal velocity it is clear that a non-linear resonance phenomenon connected with the normal vortex shedding is responsible for the observed drag increase. The drag increases are orders of magnitude larger than those predicted by a quasi-steady theory.

If the frequency corresponding to the maximum response is taken as the Strouhal frequency, then the present data show that a direct extension of the empirical equation of reference 31 is justified for Reynolds numbers in the range $700 < Re < 3000$. An extension of this work to higher Reynolds number could form the basis for vortex shedding frequency measurements which, as yet, have not been made.

Flow visualization studies show that for frequencies of oscillation within a 35% range of the natural frequency near $Re = 500$ the frequency of vortex shedding locks in to the frequency of the oscillation. This enhances our view of the effect as one of a resonance phenomenon. The oscillation is seen to

organize a wake that is disorganized by the presence of freestream turbulence and suggests that the measured drag increases are due to the increased energy fed into the vortices.

A survey of articles on bluff body drag in unsteady flow has revealed the complexity of the problem and the fact that little is known about whether a general unsteadiness can or cannot be treated in a quasi-steady manner. The present study has, unfortunately, not answered this question in general, but has shown that under certain conditions, specified here for a translational oscillation, large deviations from steady drag may be found.

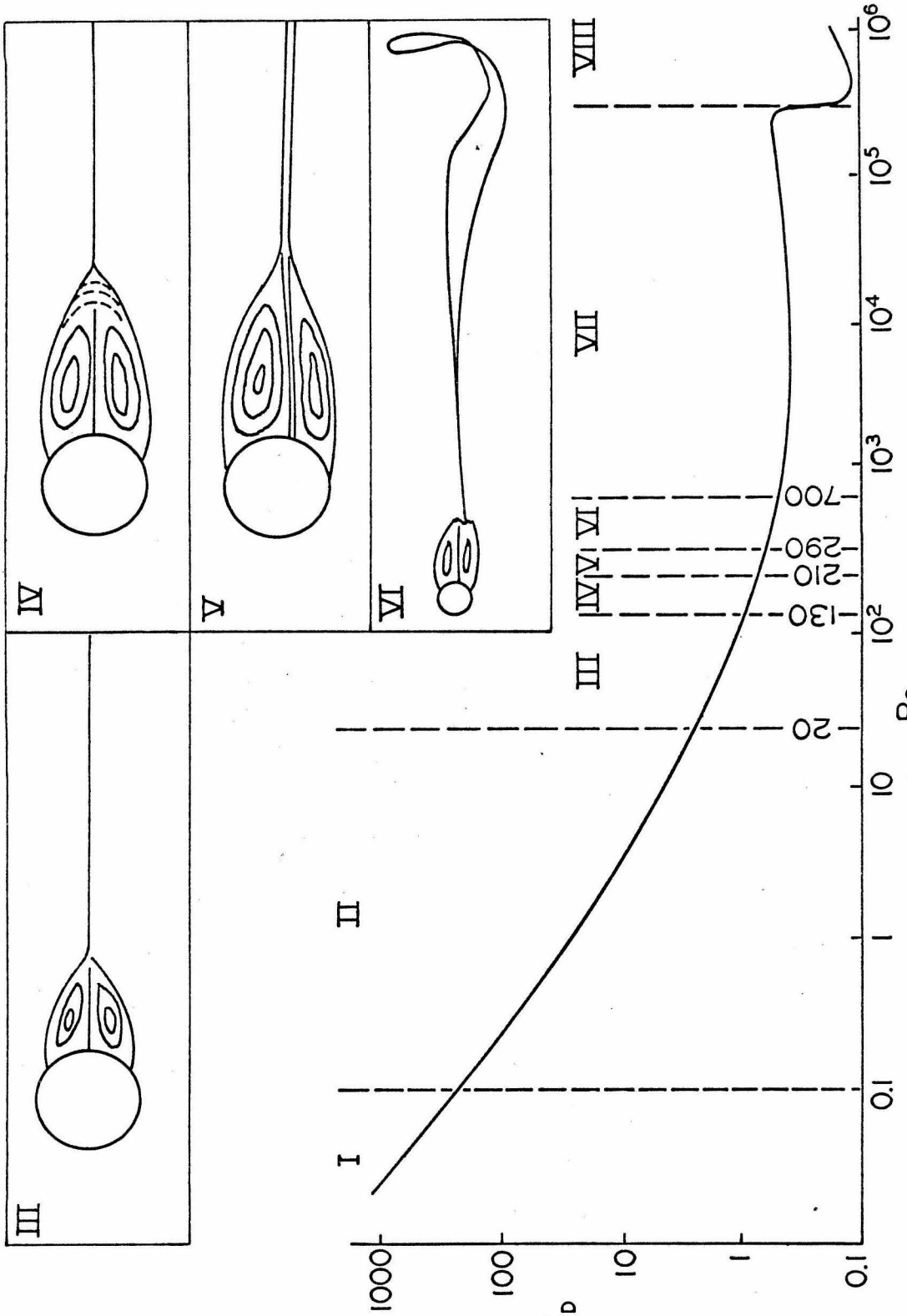

Fig. 1. The standard curve of drag coefficient vs. Reynolds number for spheres, with the Reynolds number divided into flow regimes. Inserts depict the flow in four of the regimes.

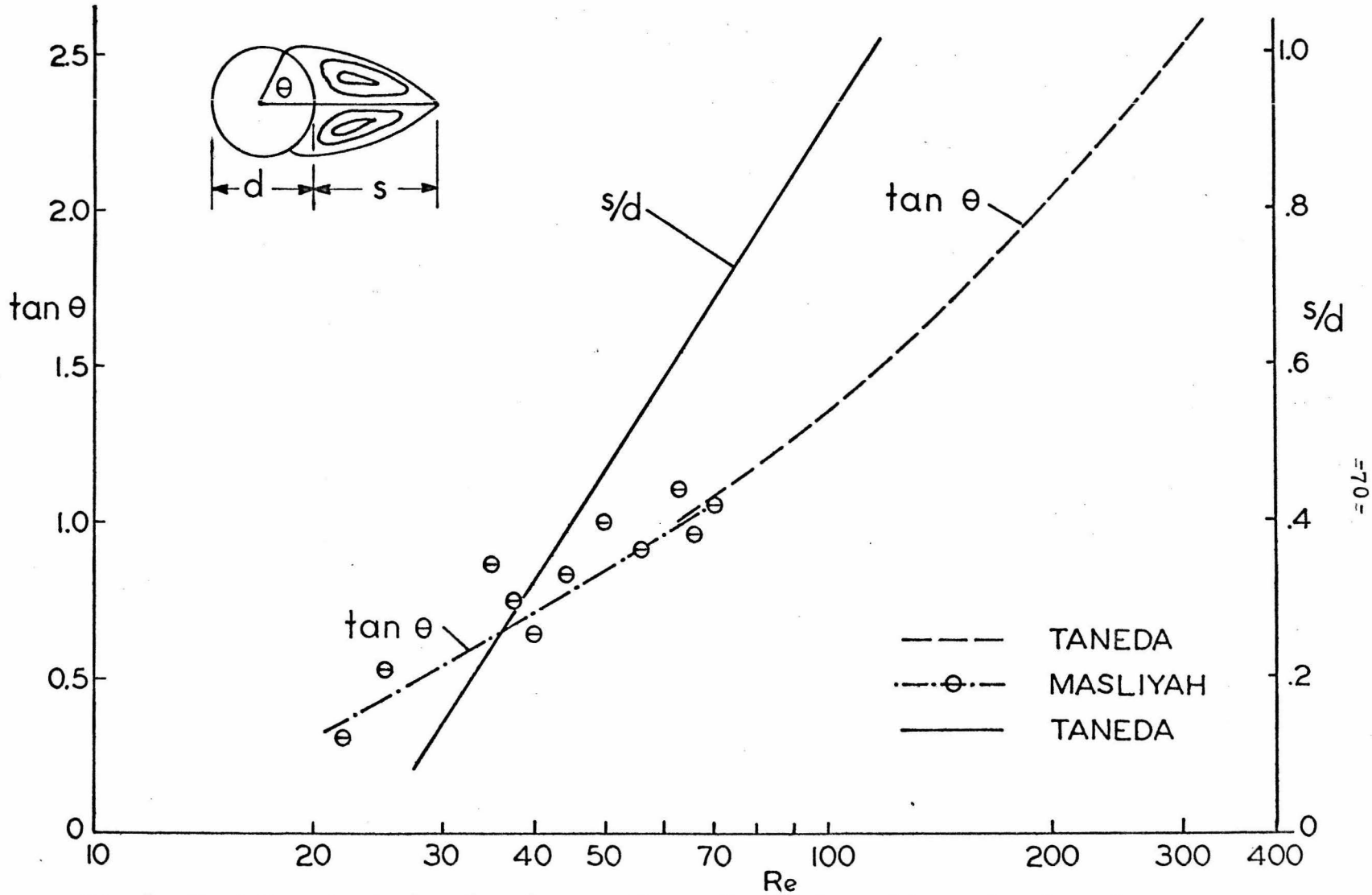

Fig. 2. Variation of wake length and separation angle with Reynolds number for spheres, from ref. 22, 28.

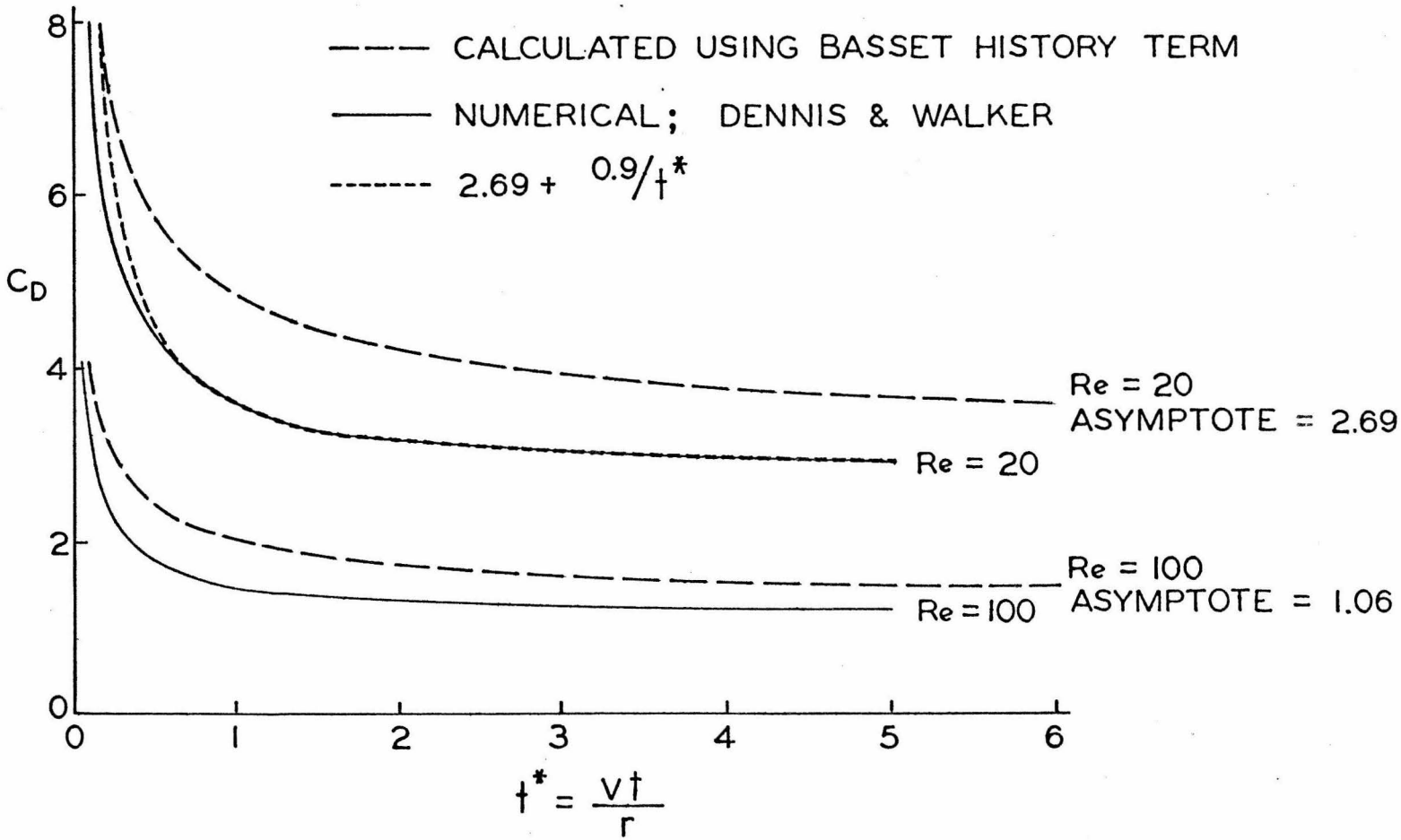

Fig. 3. The development of drag coefficient with dimensionless time for an impulsively started sphere. Numerical results from ref. 26 and an application of the Basset term are compared.

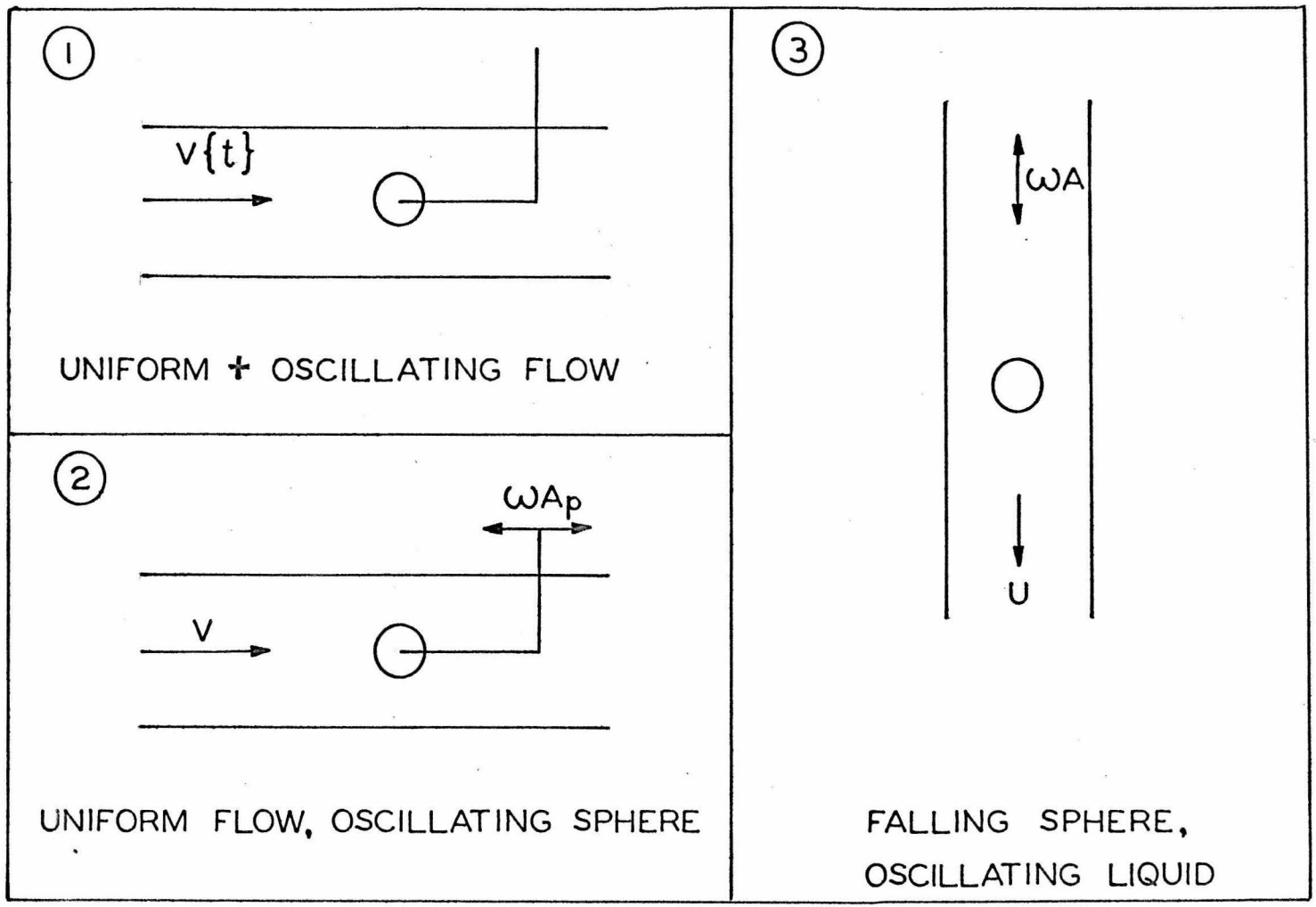

Fig. 4. Three possible experimental configurations in which sphere drag in an oscillating flow could be measured.

Fig. 5. A photograph of the apparatus showing the shaker controls (right) and the shaker and apparatus (left).

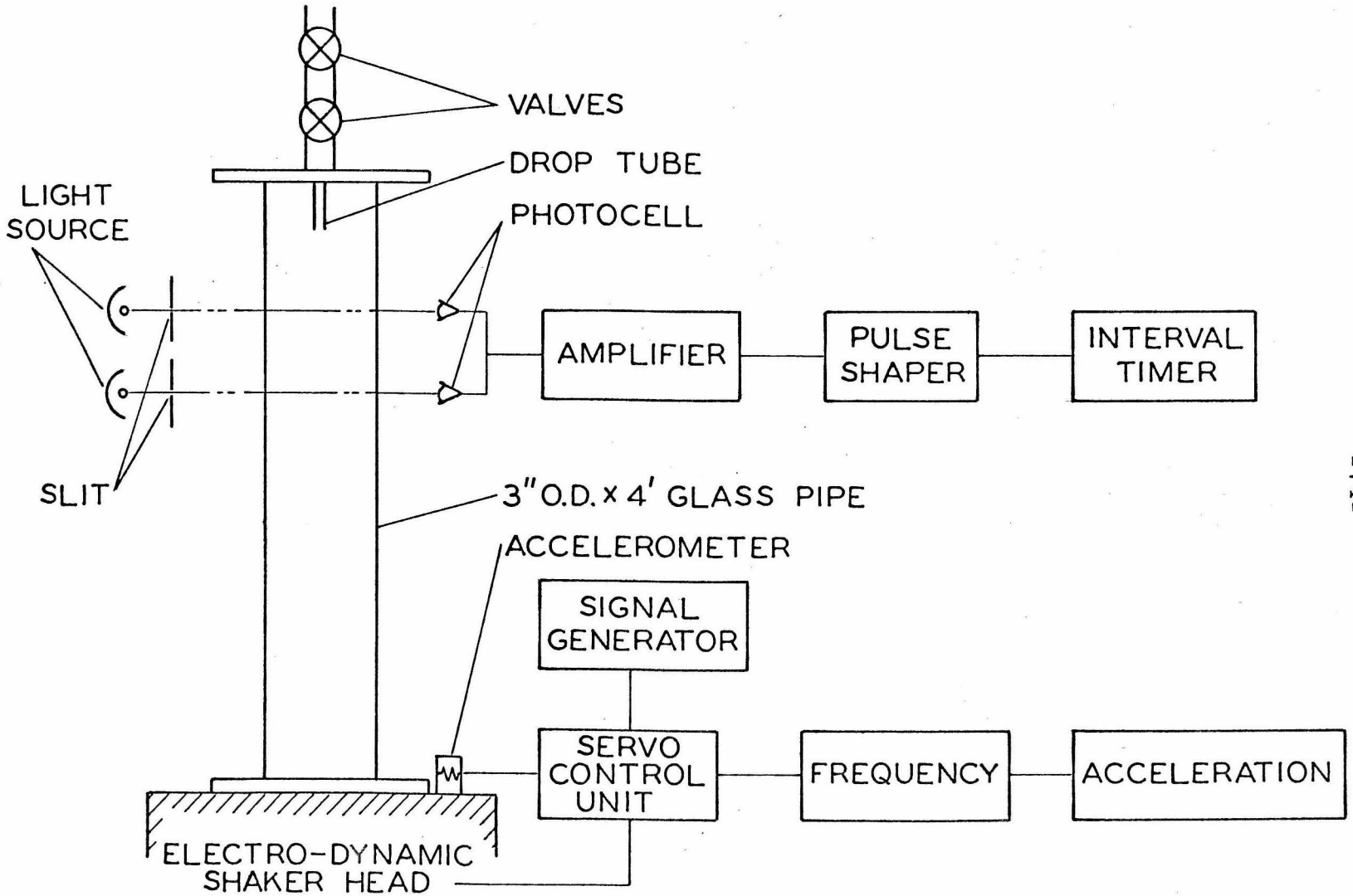

Fig. 6. A schematic diagram of the experimental apparatus used for drag measurements.

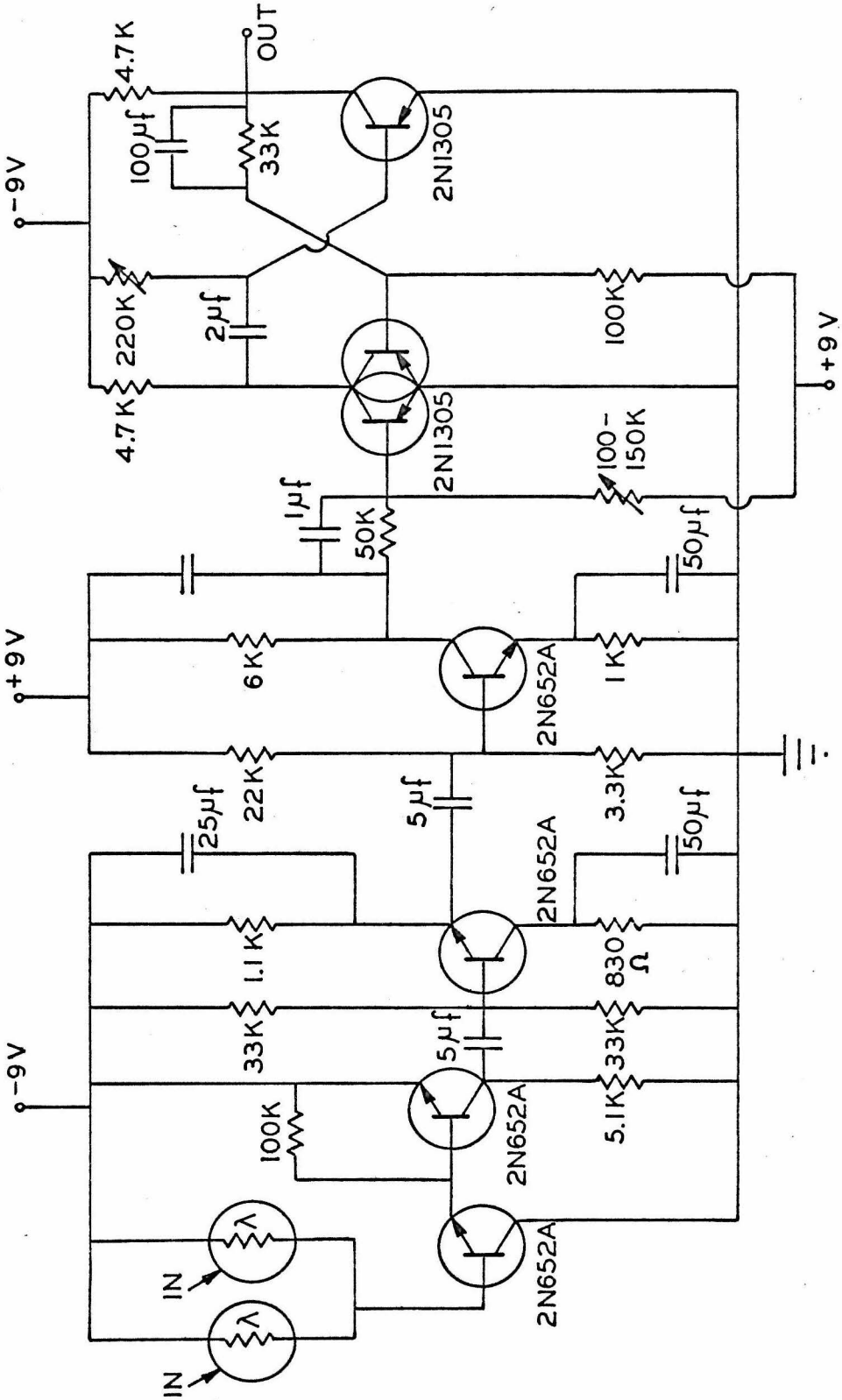

Fig. 7. Circuit diagram of the photoelectric signal conditioning device.

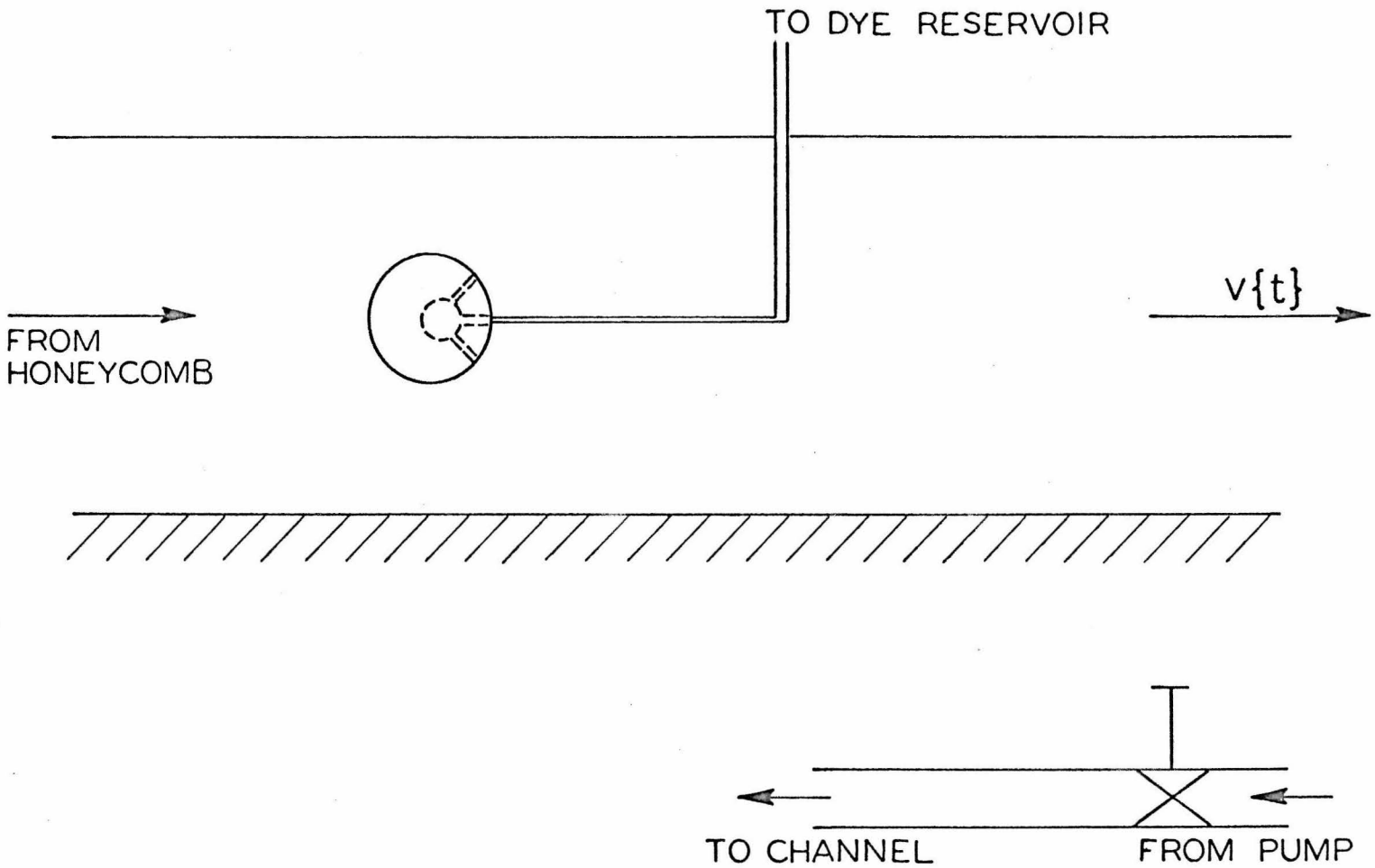

Fig. 8. A schematic diagram of the visualization apparatus in the free surface water tunnel.

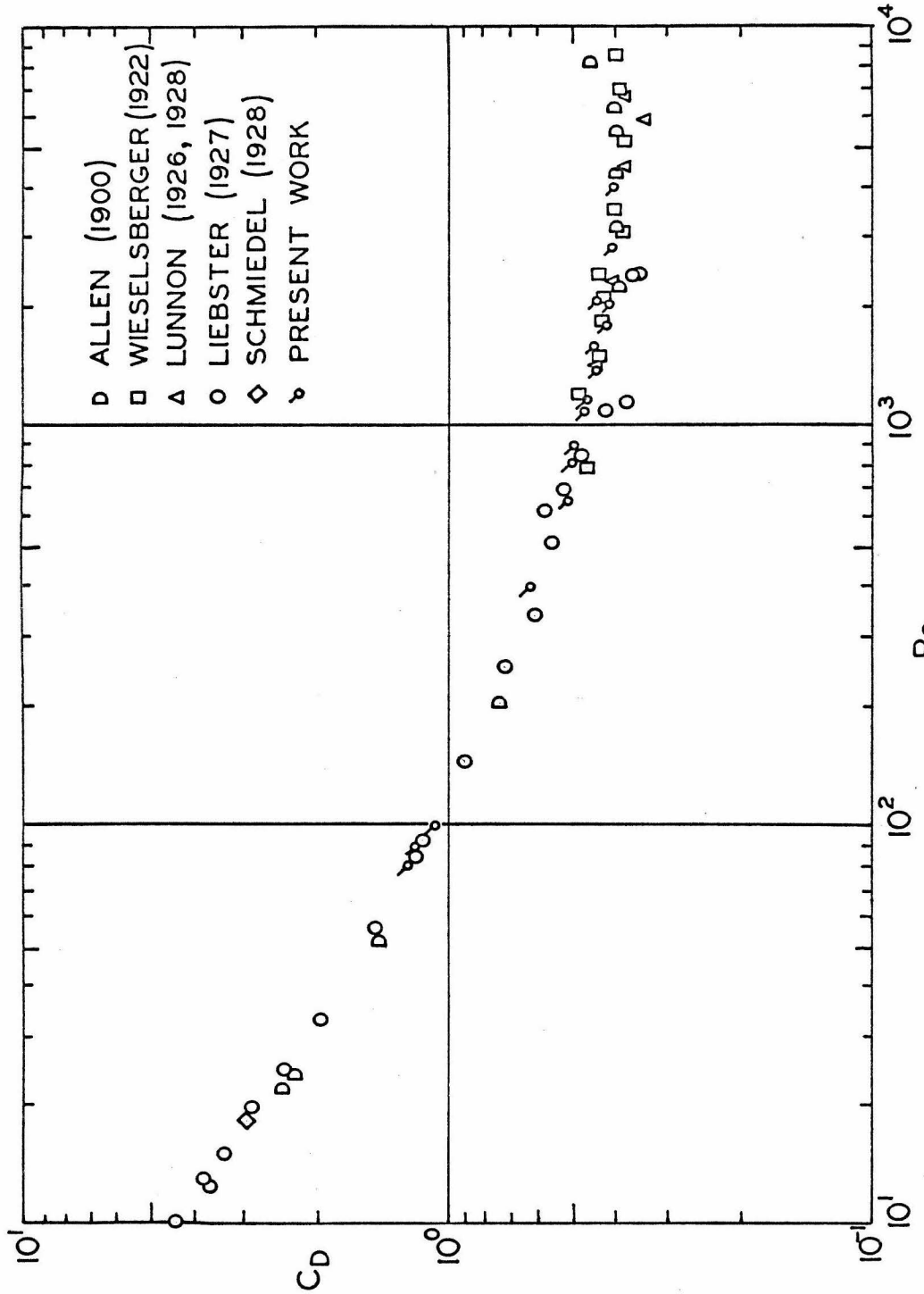

Fig. 9. Drag coefficient vs. Reynolds number, both based on the terminal velocity of spheres in a quiescent liquid. Also shown are some of the "standard" data (figure taken from figure 5 of ref. 59).

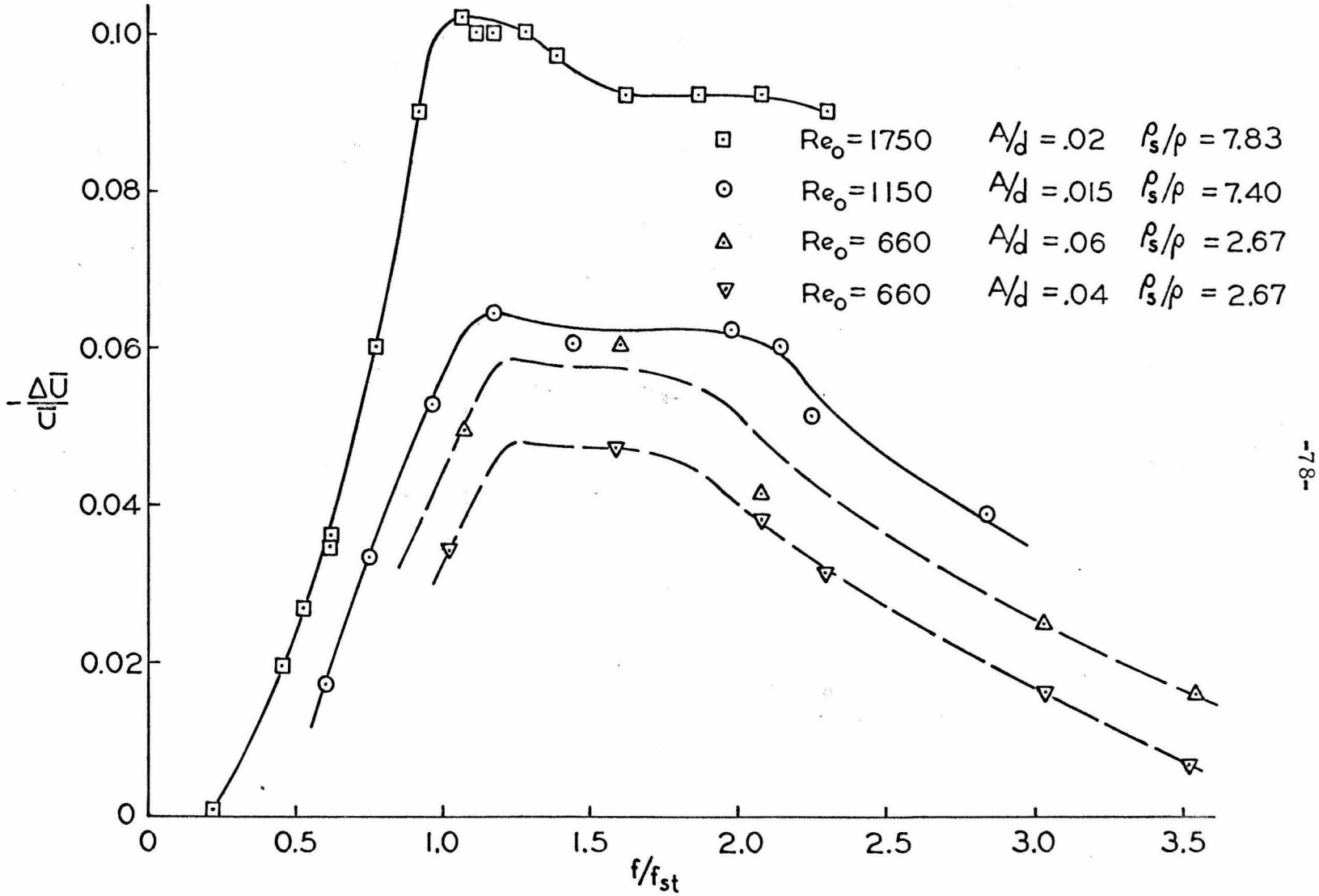

Fig. 10. Fractional change in terminal velocity vs. non-dimensional frequency for values of non-dimensional frequency up to 3.5.

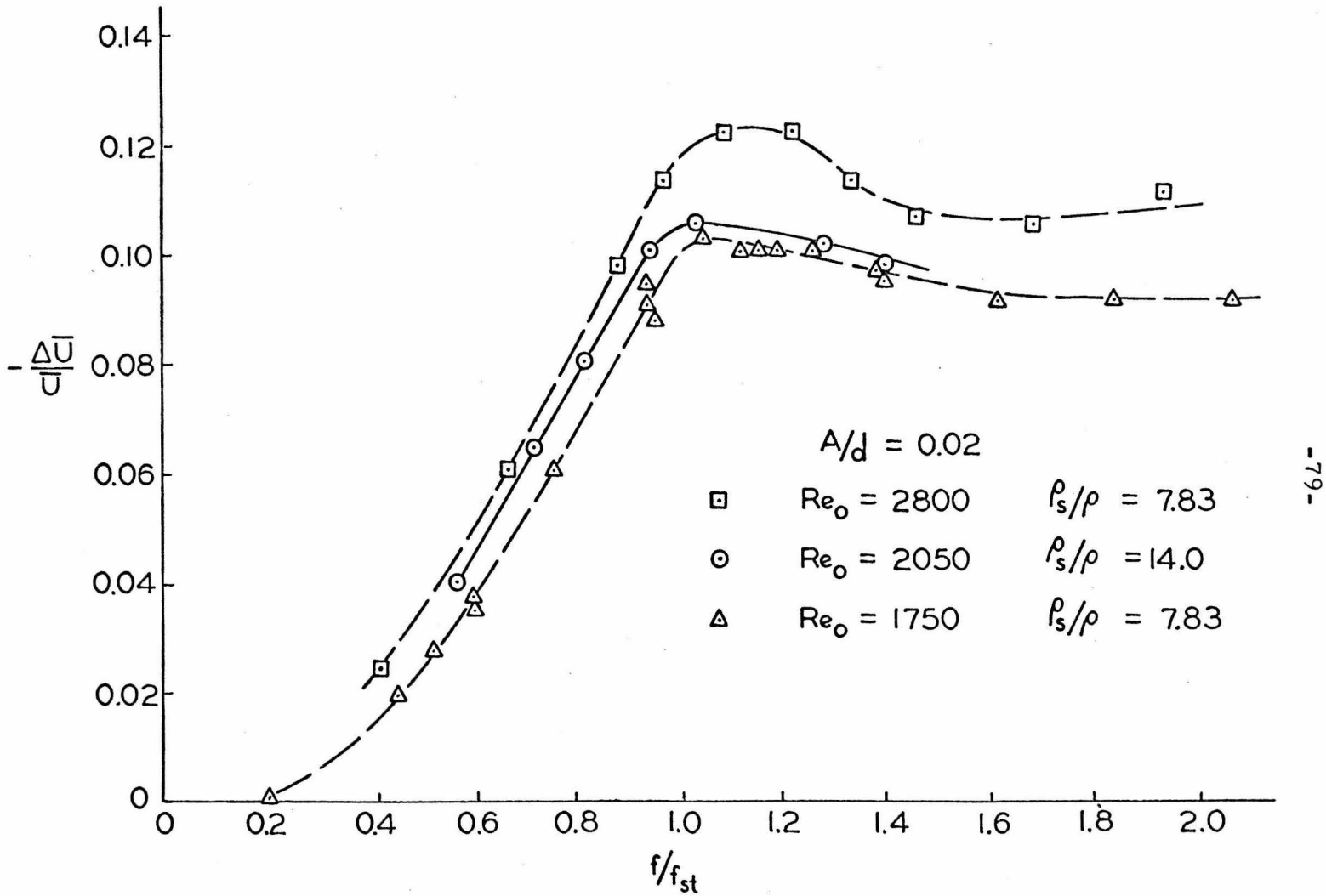

Fig. 11. Fractional change in terminal velocity vs. non-dimensional frequency for various Reynolds numbers and two density ratios.

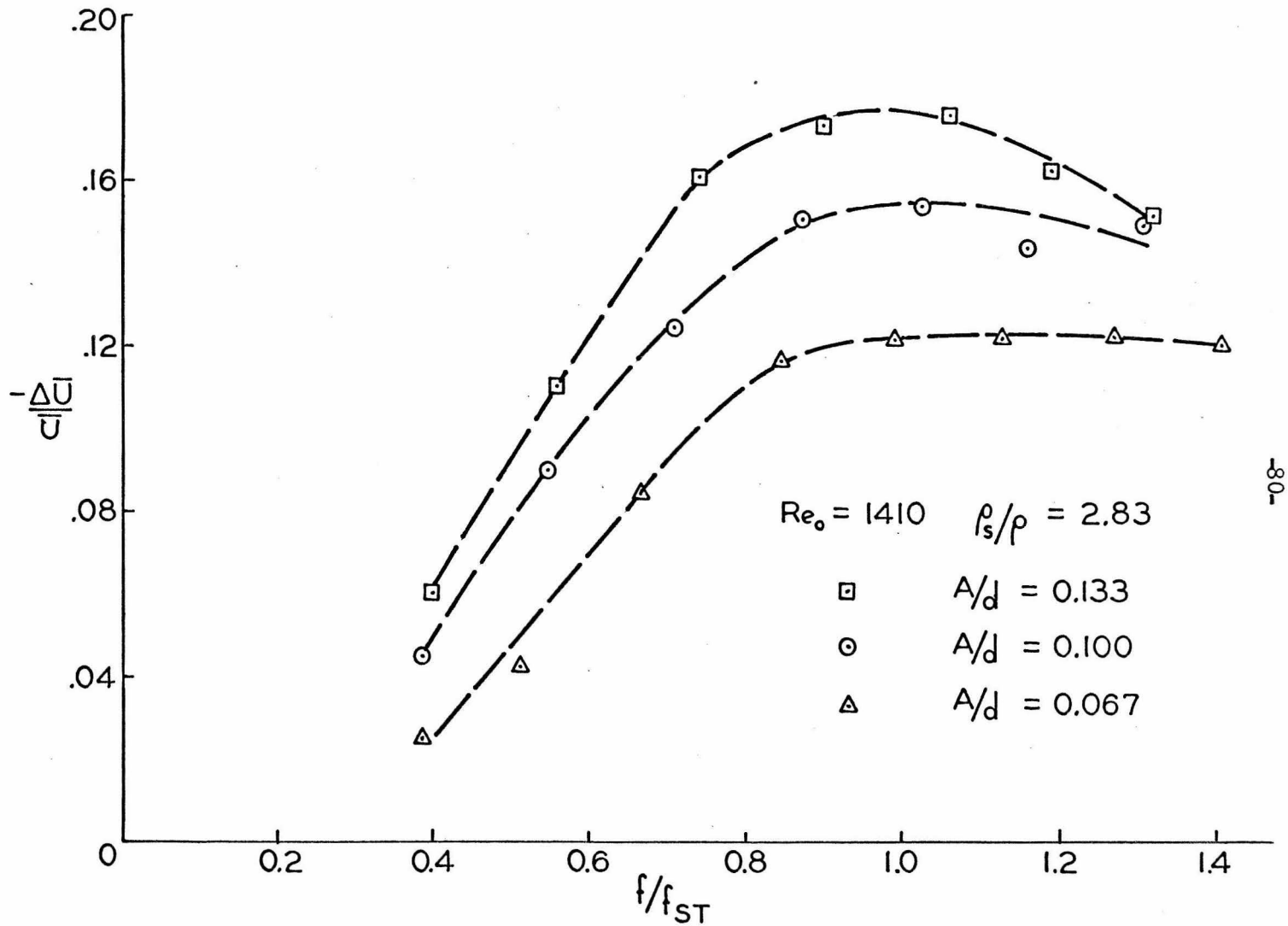

Fig. 12. Fractional change in terminal velocity vs. non-dimensional frequency, showing the effect of varying the ratio of oscillation amplitude to particle diameter.

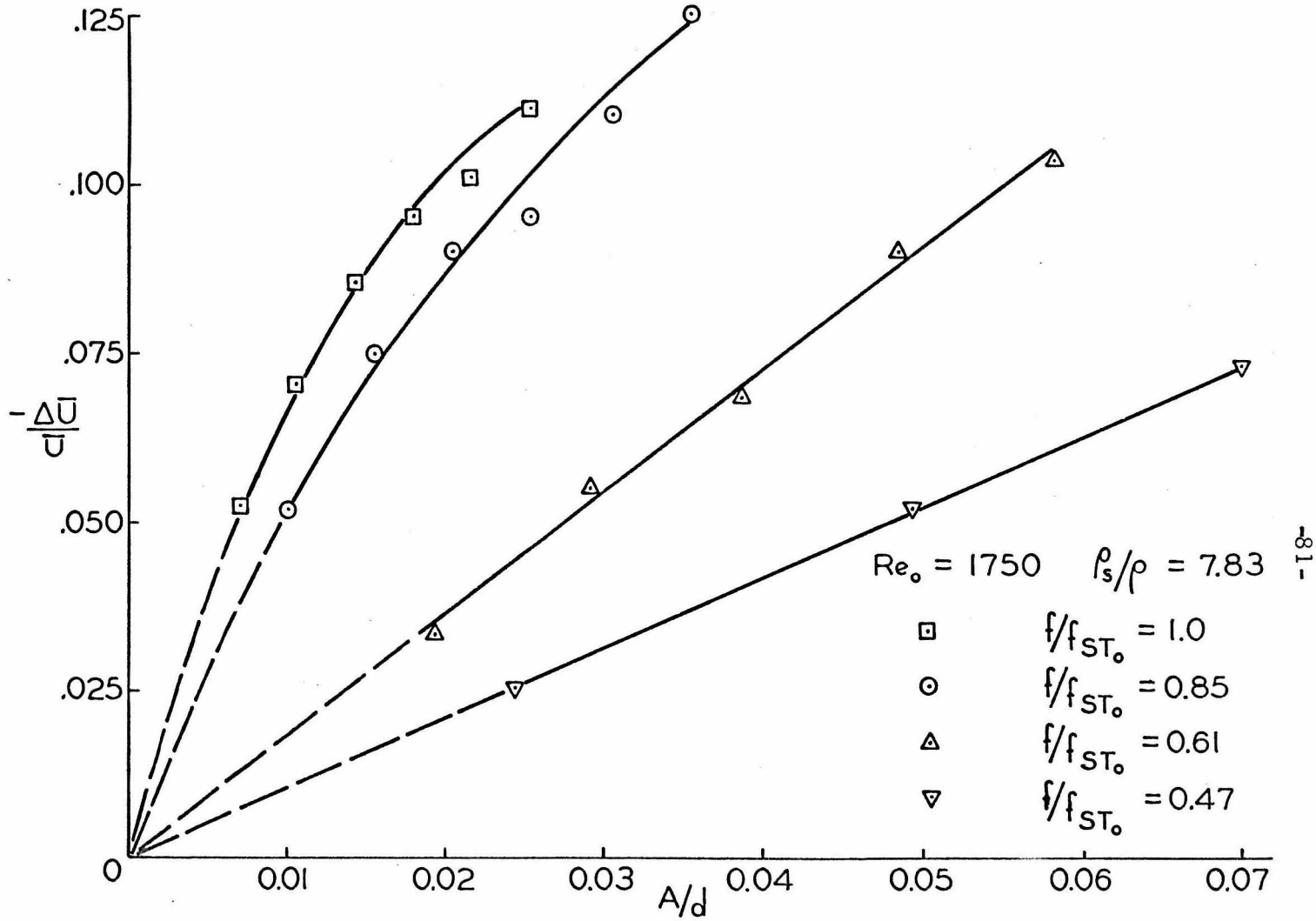

Fig. 13. The effect of amplitude ratio on terminal velocity for various ratios of oscillation frequency to undisturbed Strouhal frequency.

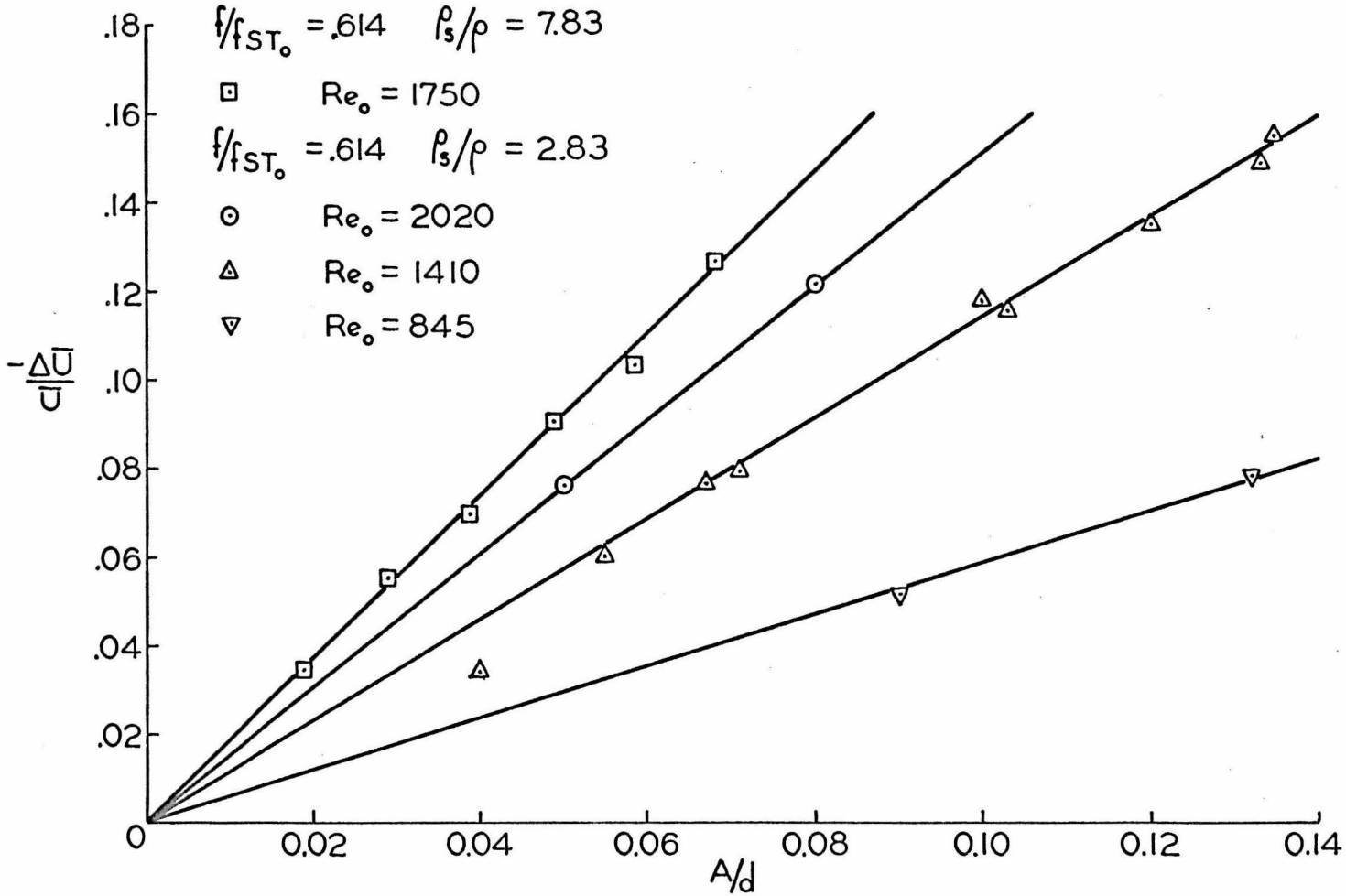

Fig. 14. Fractional change in terminal velocity vs. amplitude to diameter ratio for the ratio of oscillation frequency to undisturbed Strouhal frequency, $f/f_{ST_o} = 0.614$.

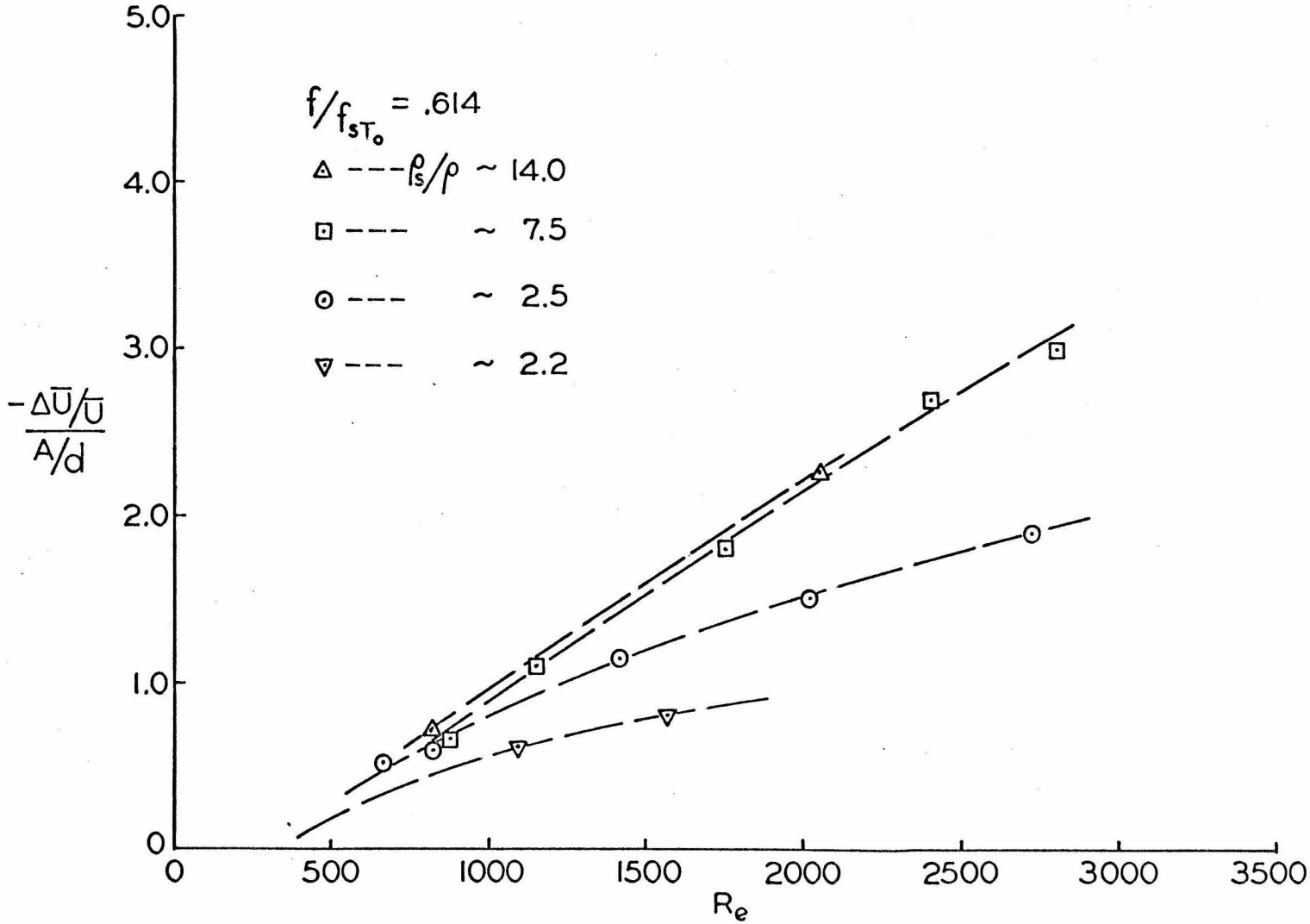

Fig. 15. Reynolds number dependence of the slope of the $-\Delta\bar{U}/\bar{U}$ vs. A/d curves at $f/f_{ST_o} = 0.614$.

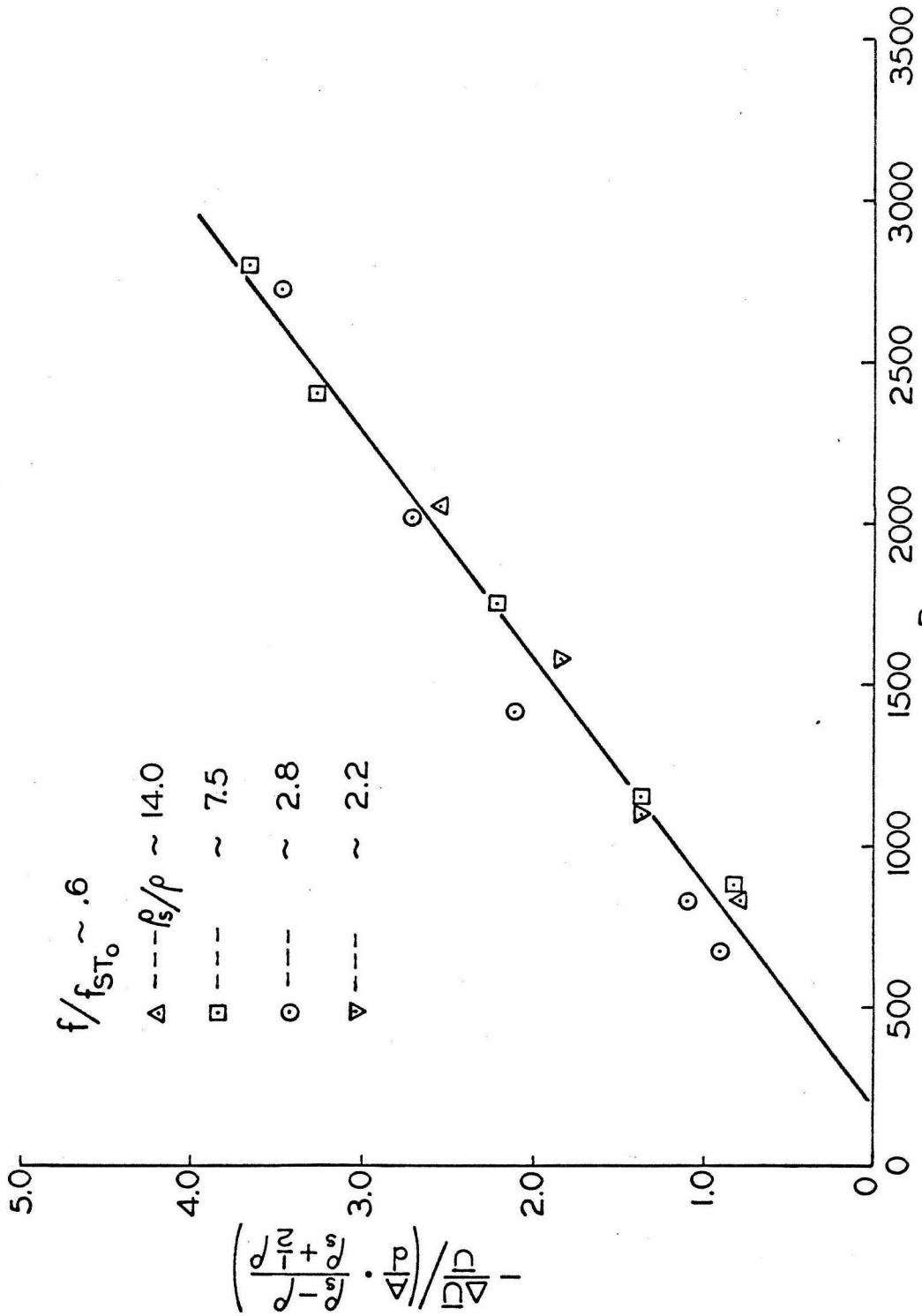

Fig. 16. The data of Fig. 15 with the effects of density ratio and amplitude ratio combined.

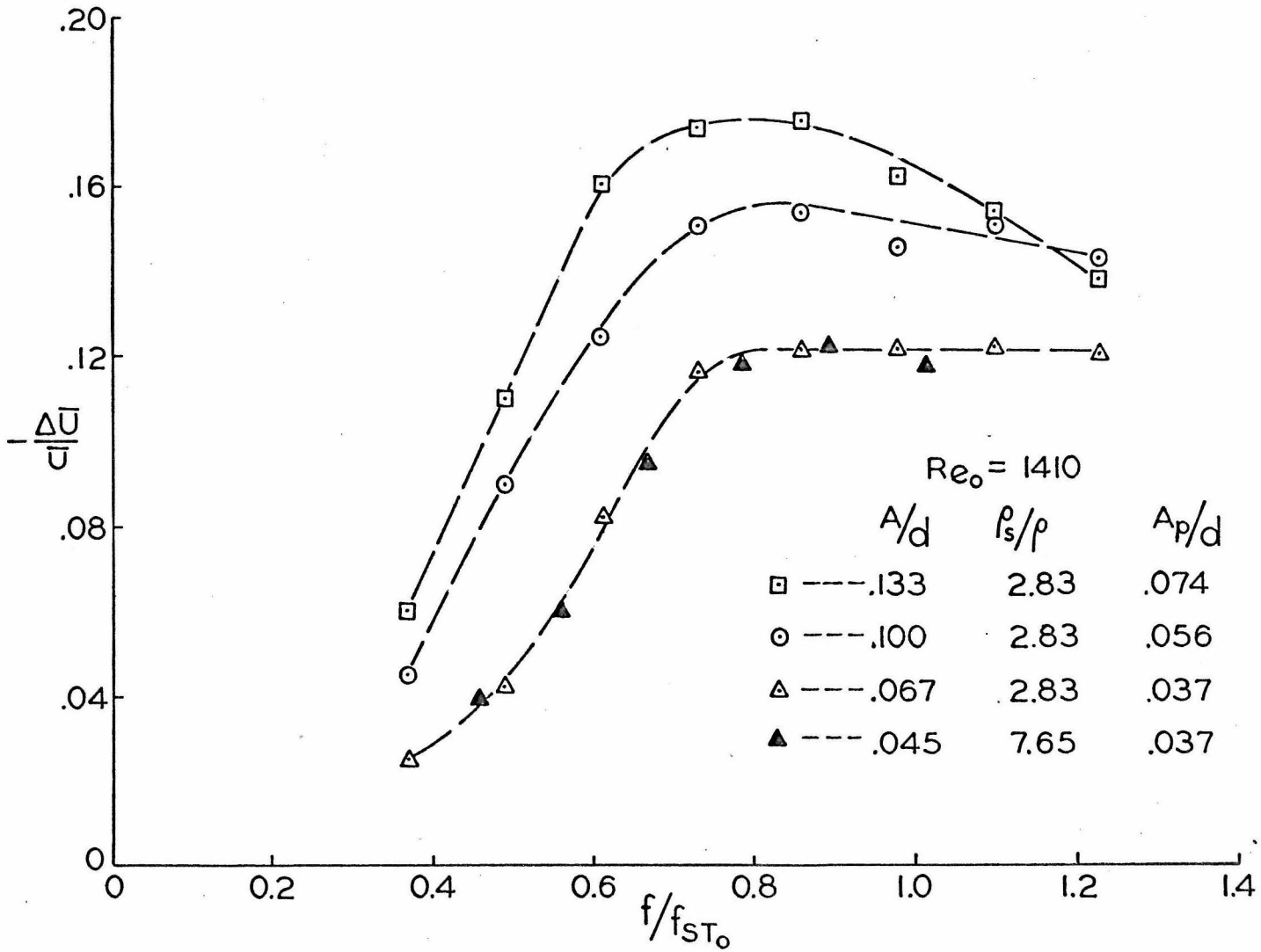

Fig. 17. The frequency dependence of the change in terminal velocity, showing the effect of the calculated amplitude relative to the particle, A_p.

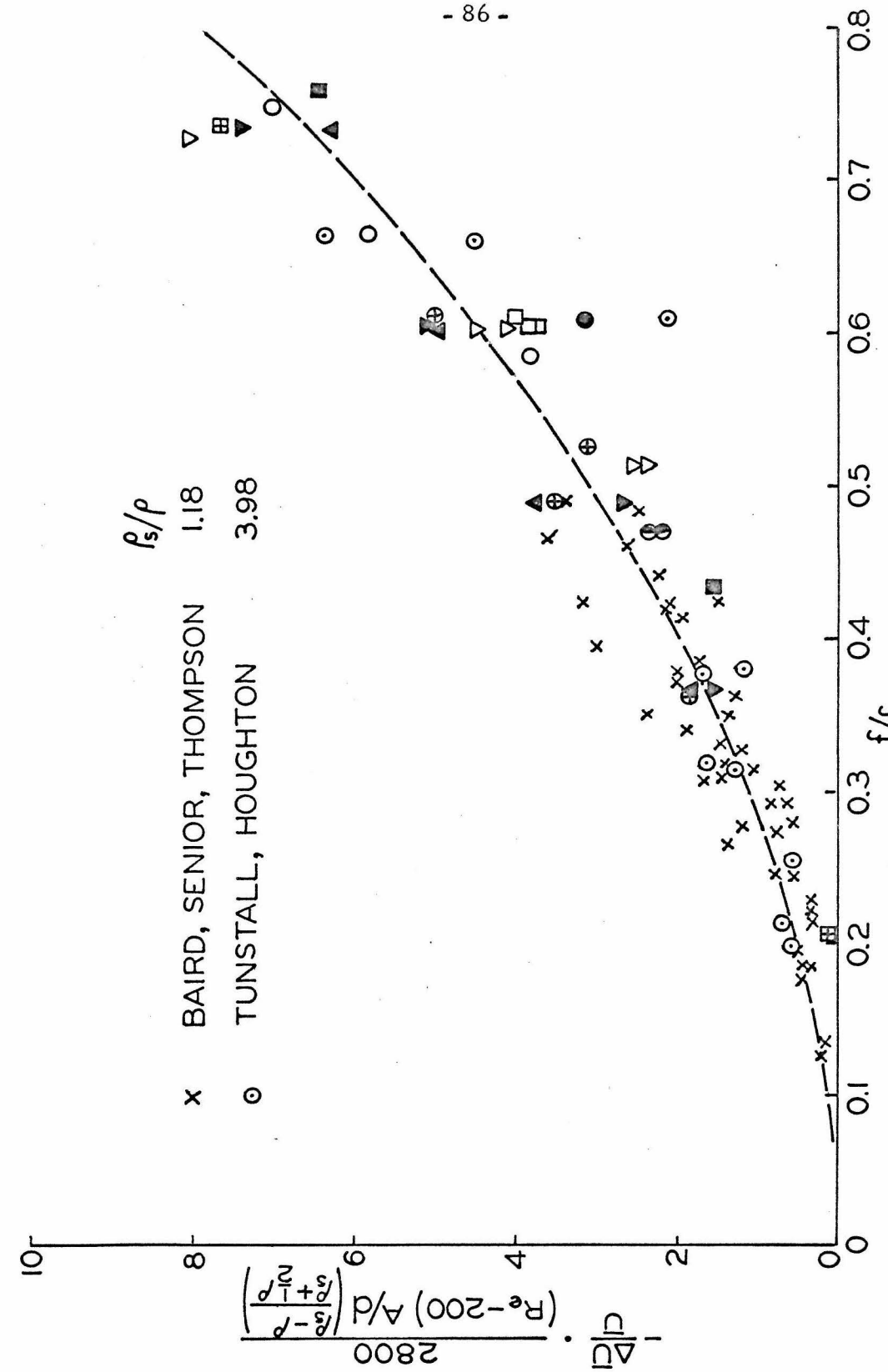

Fig. 18. Complete correlation of the data for which $f/f_{ST} \leq 0.75$. Also shown are the results from references 16 and 17.

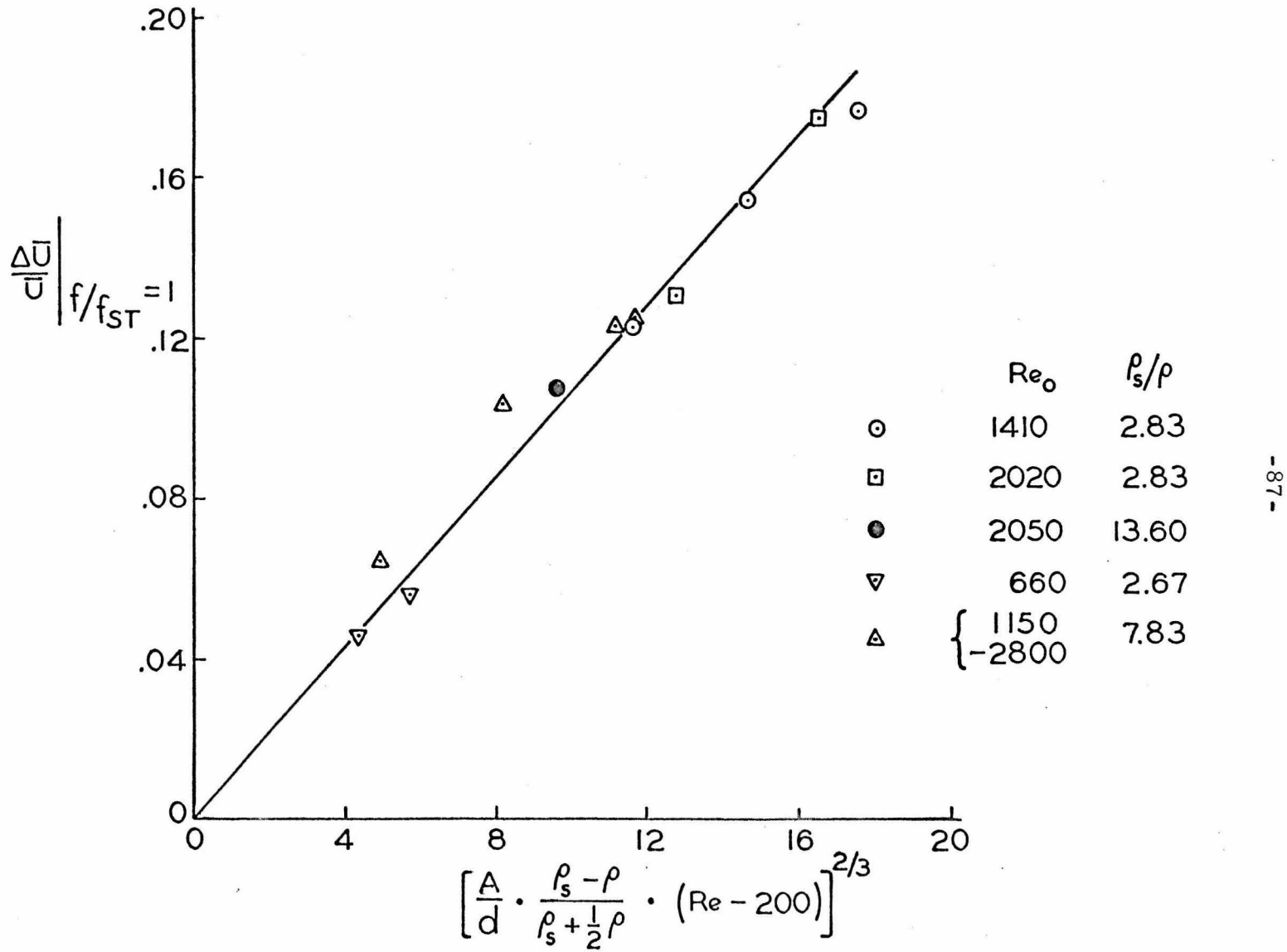

Fig. 19. Correlation of the change in terminal velocity at $f/f_{ST} \approx 1.0$ as a function Ap/d and Re.

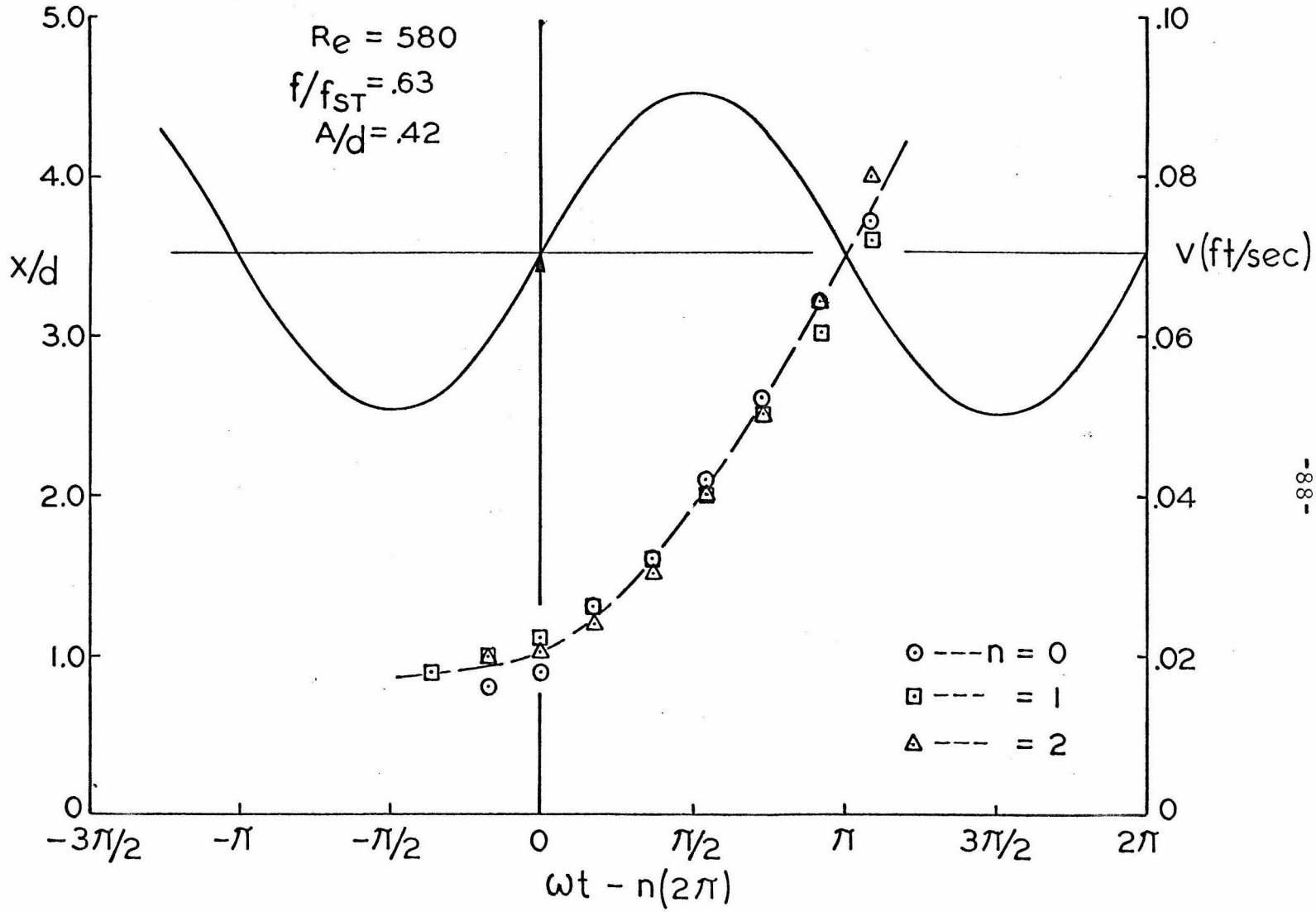

Fig. 20. Downstream position of the center of the shed vortex and the freestream velocity as a function of time for $f/f_{ST} = 0.63$.

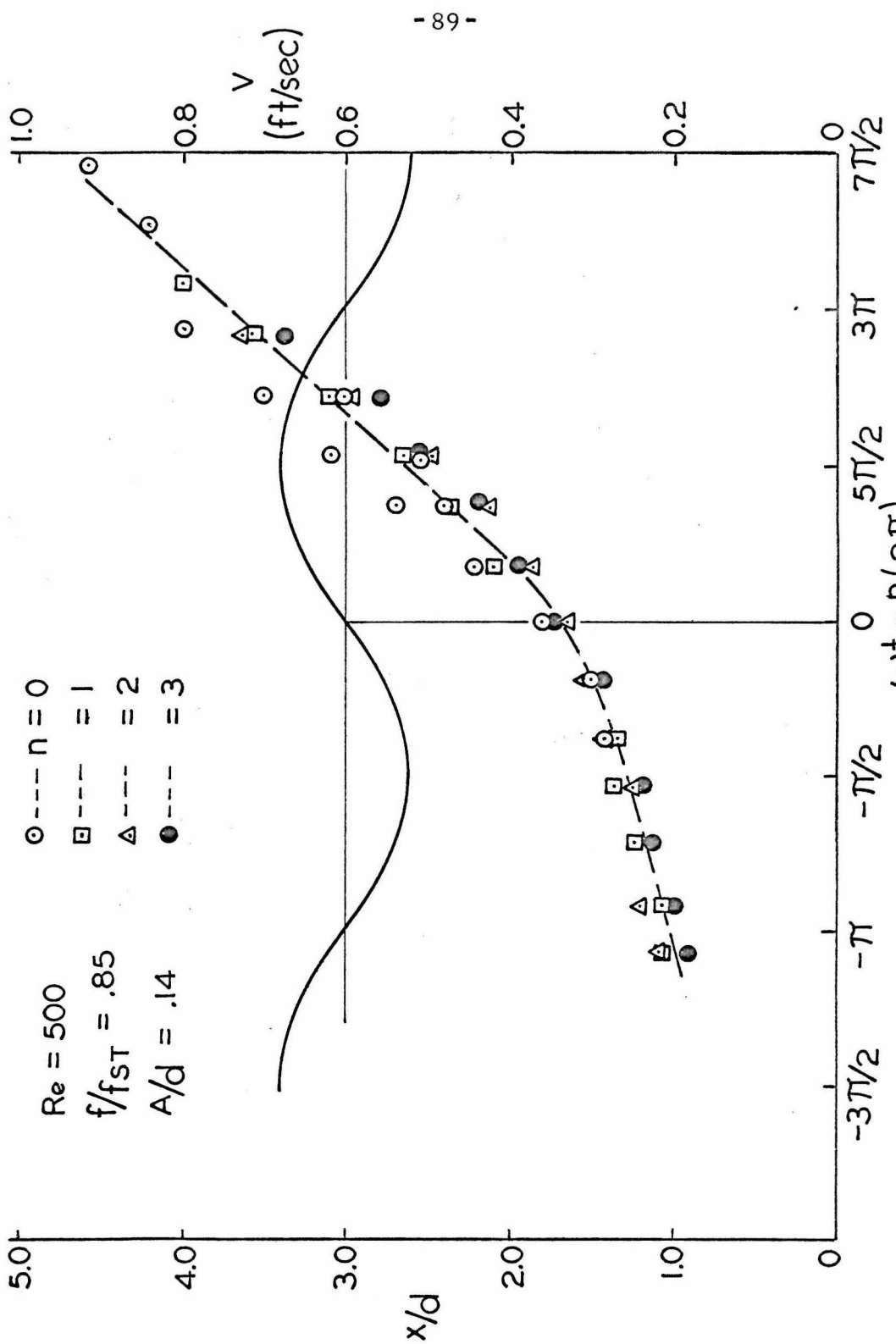

Fig. 21. Downstream position of the center of the shed vortex and the freestream velocity as a function of time for $f/f_{ST} = 0.85$.

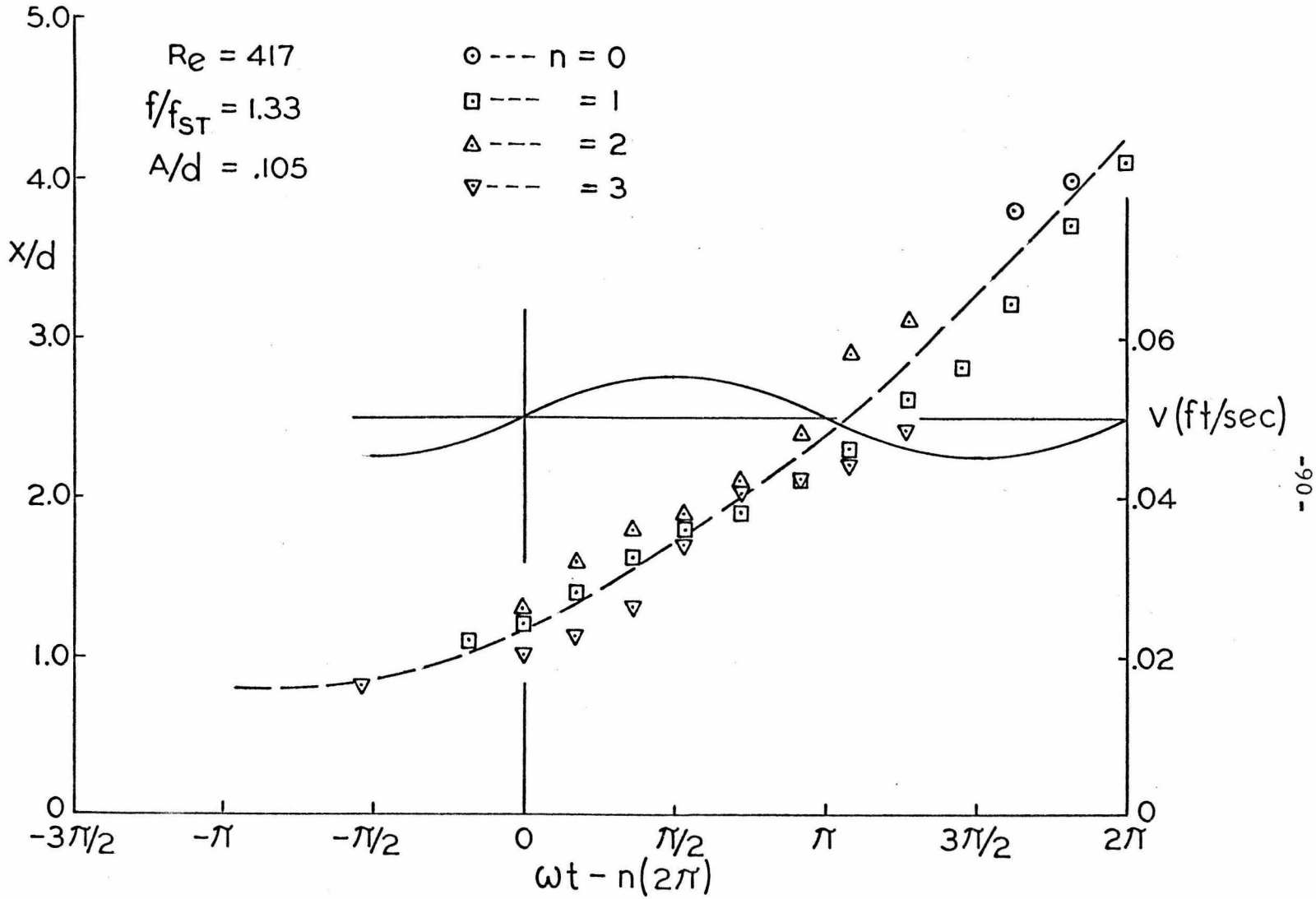

Fig. 22. Downstream position of the center of the shed vortex and the freestream velocity as a function of time for $f/f_{ST} = 1.33$.

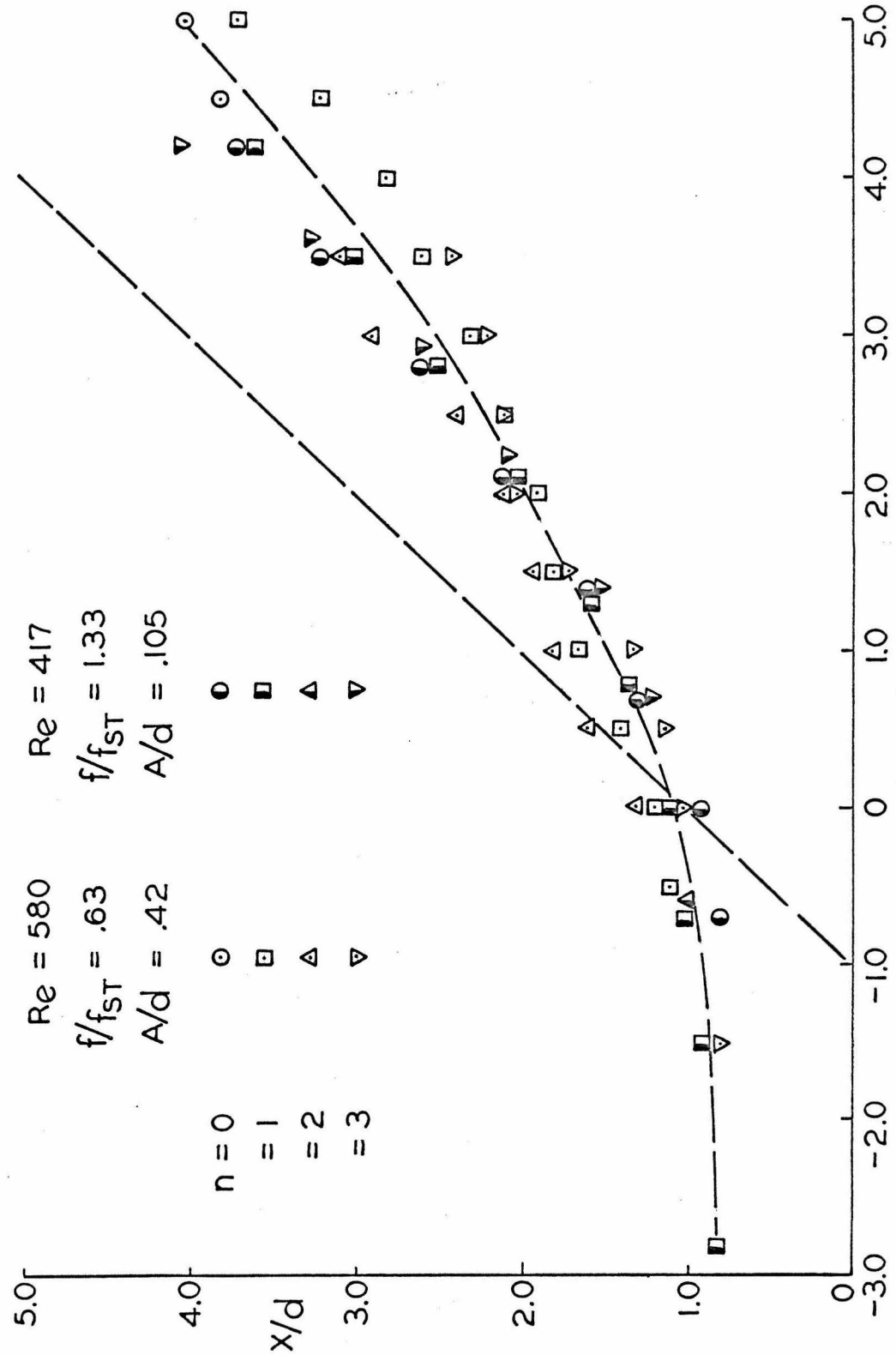

Fig. 23. Non-dimensionalization of the data of figures 20 and 22.

APPENDIX A

Experimental Conditions and Maximum Velocity Changes

In order that complete information about the dimensional variables be given, Table I lists the conditions for the free fall of the spheres with no fluid oscillation present. From the data given in the figures and from the data given in Table I it is possible to reconstruct every variable.

For example, consider the data point $-\Delta\bar{U}/\bar{U} = 0.10$ at $f/f_{ST} = 1.05$, $Re_o = 1750$, $A/d = 0.02$, $\rho_s/\rho = 7.83$ from figure 10. Table I shows that this is a 3/32 inch diameter sphere of density 7.83 in a fluid of density 1.0. The undisturbed terminal velocity U_o is 2.29 ft/sec. and the undisturbed shedding frequency is 95.5 Hz. Therefore, $\bar{U}$ is 2.08 ft/sec. and Re is 1590. Then

$$f_{ST} = .387\,(1-270/Re)\,U/d$$

$$= 85.5 \text{ Hz}$$

and f is 90.0 Hz. The amplitude of the oscillation is 2% of 3/32 inch, or 1.56×10^{-5} ft^2/sec. Thus all the variables relating to this data point have been determined.

It was not possible to show sufficient data on figure 19, regarding the peak response, that variables might be determined. For this reason, the data of the maximum effect (the effect at $f/f_{ST} = 1$) is given in Table II.

APPENDIX A

TABLE I

Terminal Conditions With No Fluid Oscillation

DIAMETER (inches)	DENSITY RATIO	TERMINAL VELOCITY (ft/sec)	REYNOLDS NUMBER	VORTEX SHEDDING FREQUENCY (cycles/sec)
1/8	2.20/1.0	1.04	1100	29.6
5/32	2.20/1.0	1.21	1570	29.7
1/8	2.83/1.06	1.18	657	25.8
3/32	2.83/1.0	1.09	845	37.0
1/8	2.83/1.0	1.36	1410	40.8
5/32	2.83/1.0	1.56	2020	40.0
3/32	7.83/1.06	2.07	885	71.2
3/32	7.83/1.02	2.23	1402	89.0
7/64	7.83/1.06	2.31	1150	75.0
3/32	7.82/1.0	2.29	1750	95.5
7/64	7.82/1.0	2.61	2350	93.5
1/8	7.83/1.0	2.74	2800	92.0
1/8	14.5/1.11	3.29	825	82.2
1/8	14.5/1.06	3.71	2050	120

APPENDIX A

TABLE II

Terminal Velocity Changes at $f/f_{ST}=1$

$\frac{\rho_s}{s}$	$\frac{A}{d}$	Re_o	$\frac{\Delta\bar{U}}{\bar{U}}$	$[\frac{A_p}{d}(Re-200)]^{2/3}$
2.83	.067	1410	.123	11.6
2.83	.100		.155	14.7
2.83	.133		.176	17.5
2.83	.053	2020	.130	12.8
2.83	.08		.175	16.5
14.5	.02	2050	.107	9.6
7.40	.015	1150	.065	4.9
7.83	.02	1750	.104	8.1
7.83	.02	2800	.123	11.2
2.67	.06	660	.055	5.75
2.67	.04	660	.045	4.4
7.65	.045	1410	.123	11.6

APPENDIX B

Equivalence of Three Different Experiments

Consider the three experiments mentioned in Chapter 3. These experiments are described in figure 4.

Experiment 3 $\Leftrightarrow$ experiment 2

The equivalence of these experiments when $\rho_s/\rho \to \infty$ in 3 is most easily shown. The comparison must be made, of course, with Re, A/d, and f/f_{ST} held fixed. The equation of motion for the particle is

$$m_s \frac{dU}{dt} = (m_s - m)g + m\dot{V} - D$$

Consider first the mean flow, for which

$$(m_s - m)g = 3/4\,(C_{\bar{D}}/d)\, m\, \bar{U}^2$$

Therefore, in order that $\bar{U}$ be constant while $\rho_s \to \infty$, we let

$$g \to 0$$

such that

$$(m_s - m)\, g/m = \text{constant}$$

Hence the experiments may be compared with all variables the same, i. e., mean velocity, diameter, kinematic viscosity, fluid density, amplitude and frequency. Then the fluctuating terms will give

$$m_s \frac{dU}{dt} = m\dot{V} - D'$$

where D' is the fluctuating part of the drag. But, whatever the fluctuating part of the drag is, it is proportional to the fluid density and it is finite. Therefore, as m is becoming finite, we must have

$$\frac{dU}{dt} \rightarrow 0$$

in the steady state. So the infinite density sphere does not respond to the fluctuating fluid forces on it and sees a freestream velocity with a mean $\overline{U}$ and an oscillation of amplitude A. This is identical to a sphere supported in a tunnel except for the presence of the gravitational pressure gradient.

It is simple to show that the superposition of a gravitational field in an incompressible flow where only kinematic conditions are to be satisfied on the body does not affect the flow field. In experiment 2 the relevant equations are

$$\nabla \cdot \underline{V} = 0$$

$$\frac{\partial \underline{V}}{\partial t} + \underline{V} \cdot \nabla \underline{V} = -\frac{1}{\rho} \nabla p + \nu \nabla^2 \underline{V}$$

In experiment 3 the relevant equations are, relative to the infinite density sphere

$$\nabla \cdot \underline{V} = 0$$

$$\frac{\partial \underline{V}}{\partial t} + \underline{V} \cdot \nabla \underline{V} = -\frac{1}{\rho} \nabla (p + \phi) + \nu \nabla^2 \underline{V}$$

where ϕ is the gravitational potential $\rho g z$.

The boundary condition on $\underline{V}$ are the same in both, and the boundary condition on p in 2 is the same as that on $(p+\phi)$ in 3. Therefore, depending only on the uniqueness of this differential equation, the flow fields in these two experiments are identical. The forces on the spheres differ, of course, by the integral of ϕ around the body, i.e., by the buoyancy.

Experiment 1 $\Leftrightarrow$ experiment 2

If a coordinate frame moves with the sphere in experiment 1, then the motion of the fluid looks identical to that in experiment 2. This frame is an accelerating one and a correction must be made for this. From relativity theory, an accelerating frame is indistinguishable from an inertial frame in a gravitational field.

By comparison with the previous arguments then, the flow fields in experiments 1 and 2 are identical and the forces differ only by the effect of the oscillating pressure gradient necessary to support the fluid motion in experiment 2. The mean forces are, of course, the same.

REFERENCES

1. Haas, Roger A., "Particle Kinetics of Gas-Solid Particle Mixtures," Ph. D. Thesis, California Institute of Technology (1969).

2. Willus, Charles, A., "An Experimental Investigation of Particle Motion in Fluidized Beds," Ph. D. Thesis, California Institute of Technology (1970).

3. Khudiakow, G. N., Izvest, Akad. Nauk. SSSR, Otdel. Tekh. Nauk., 7, (1953), p. 1022.

4. Torobin, L. B., Gauvin, W. H., "The Drag Coefficients of Single Spheres Moving in Steady and Accelerated Motion in a Turbulent Fluid," A. I. Ch. E. Journal, 7, (1961). pp. 615-619.

5. Tchen, C. M., "Mean Value and Correlation Problems Connected with the Motion of Small Particles in a Turbulent Fluid," Dissertation, University of Delft (1947), Pub. Martinus Nijhoff.

6. Corrsin, S., Lumley, J. L., "On the Equations of Motion for a Particle in Turbulent Fluid," Appl. Sci. Res. A., VI, (1956), pp. 114-116.

7. Lumley, J. L., "Some Problems Connected with the Motion of Small Particles in Turbulent Fluid," Ph. D. Thesis, Department of Aeronautics, The Johns Hopkins University (1957).

8. Magarvey, R. H., Bishop, Roy L., "Transition Ranges for Three-dimensional Wakes," Can. J. Phys., 39 (1961), pp. 1418-1422.

9. Roshko, A., "Experiments on the Flow Past a Cylinder at Very High Reynolds Number," J. Fluid Mech., 10 (1961), p. 345.

10. Rudinger, G., "Effective Drag Coefficient for Gas-Particle Flow in Shock Tubes," ASME Paper No. 69-WA/FE-21 (1969).

11. Willmarth, W. W., Enlow, R. L., "Aerodynamic Lift and Moment Fluctuations of a Sphere," J. Fluid Mech., 36, (1969), pp. 417-432.

12. Zarin, N. A., Nicholls, J. A., "Sphere Drag in Solid Rockets--Non-Continuum and Turbulence Effects", Comb. Sci. and Tech., 3 (1971), pp. 273-285.

13. Roos, F. W., Willmarth, W. W., "Some Experimental Results on Sphere and Disk Drag," AIAA Journal, 9 (1971), p. 285-291.

14. Kendall, J. M., Jr., "The Periodic Wake of a Sphere", JPL Space Programs Summary, 4 (1964), pp. 251-252.

15. Hamilton, W. S., Lindell, J. E., "Fluid Force Analysis and Accelerating Sphere Tests", J. Hyd. Div. ASCE, 97 (1971), pp. 805-816.

16. Baird, H. M. I., Senior, M. G., Thompson, R. J., "Terminal Velocities of Spherical Particles in a Vertically Oscillating Liquid," Chemical Engineering Science, 22, Pergamon Press (1967), pp. 551-558.

17. Tunstall, E. G., Haughton, G., "Retardation of Falling Spheres by Hydrodynamic Oscillations," Chemical Engineering Science, 23 (1968), pp. 1067-1081.

18. Khudiakow, G. N., Chukhanov, Z. F., Doklady Akad. Nauk, SSSR, 78 (1951), p. 681.

19. Torobin, L. B., Gauvin, W. H., "Turbulent Flow Ballistic Facility for Particle Momentum Transfer Studies," A. I. Ch. E. Journal, 7, (1961), pp. 406-410.

20. Clamen, A., Gauvin W. H., "Effects of Turbulence on the Drag Coefficients of Spheres in a Supercritical Flow Regime", A. I. Ch. E. Journal, 15 (1969), pp. 184-189.

21. Torobin, L. B., Gauvin, W. H., "Fundamental Aspects of Solids-Gas Flow, Part II. The Sphere Wake in Steady Laminar Fluids", Can. J. Chem. Eng., 37 (1959), pp. 167-176.

22. Taneda, S., "Experimental Investigation of the Wake Behind a Sphere at Low Reynolds Numbers", J. Phys. Soc. Japan, 11 (1956), pp. 1104-1108.

23. Nisi, H., Porter, A. W., "On Eddies in Air", Phil. Mag., 46 (1923), pp. 754-768.

24. Rimon, Y., Cheng, S. I., "Numerical Solution of a Uniform Flow over a Sphere at Intermediate Reynolds Numbers", Phys. Fluids, 12 (1969), pp. 949-959.

25. Masliyah, J. H., Epstein, N., "Comments on 'Numerical Solution of a Uniform Flow over a Sphere at Intermediate Reynolds Numbers'", Phys. Fluids, 14 (1971), pp. 750-752.

26. Dennis, S. C. R., Walker, J. D. A., "Numerical Solutions for Time-Dependent Flow Past an Impulsively Started Sphere", Phys. of Fluids, 15 (1972), pp. 517-525.

27. Jensen, V. G., "Viscous Flow Round a Sphere at Low Reynolds Numbers", Proc. Roy. Soc., A249 (1959), pp. 346-366.

28. Masliyah, J. H., "Steady Wakes Behind Oblate Spheriods: Flow Visualization", Phys. of Fluids, 15 (1972), pp. 1144-1146.

29. Pruppacher, H. R., LeClair, B. P., Hamielec, A. E., "Some Relation Between Drag and Flow Pattern of Viscous Flow past a Sphere and Cylinder at Low and Intermediate Reynolds Numbers", J. Fluid Mech., 44 (1970), pp. 781-790.

30. Masliyah, J. H., Epstein, N., "Numerical Study of Steady Flow Past Spheriods", J. Fluid Mech., 44 (1970), pp. 493-512.

31. Goldberg, A., Florsheim, B. H., "Transition and Strouhal Number for Incompressible Wake of Various Bodies", Phys. of Fluids, 9 (1966), p. 45-50.

32. Magarvey, R. H., Bishop, R. L., "Wakes in Liquid-Liquid Systems", Phys. of Fluids, 4, (1961), pp. 800-805.

33. Möller, W., "Experimentelle Untersuchengen zur Hydrodynamik der Kugel," Z. Physik, 39 (1938), pp. 58-80.

34. Abraham, F. F., "Functional Dependence of Drag Coefficient of a Sphere on Reynolds Number", Phys. of Fluids, 13, (1970), pp. 2194-2195.

35. Torobin, L. B., Gauvin, W. H., "Fundamental Aspects of Solids-Gas Flow, Part III: Accelerated Motion of a Particle in a Fluid", Can. J. Chem. Eng., 38 (1960), pp. 142-153.

36. Sarpkaya, T., Garrison, C. J., "Vortex Formation and Resistance in Unsteady Flow", J. App. Mech., 30 (1963), pp. 16-24.

37. Chen, C. F., Ballengee, David B., "Vortex Shedding from Circular Cylinders in an Oscillating Free Stream," AIAA Journal 9, (1971), pp. 340-342.

38. Honji, H., Taneda, S., "Unsteady Flow past a Circular Cylinder", J. Phys. Soc. Japan, 27 (1969), pp. 1668-1677.

39. Tatsuno, M., Taneda, S., "Visualization of the Unsteady Flow Past Cylinders and Plates Decelerated from a Steady Speed", J. Phys. Soc. Japan, 31 (1971), pp. 1266-1274.

40. Ingebo, R. D., "Drag Coefficients for Droplets and Solid Spheres in Clouds Accelerating in Airstreams", NACA Technical Note, NASA TN 3762 (1956).

41. Keulegan, G. H., Carpenter, L. H., "Forces on Cylinders and Plates in an Oscillating Fluid", J. Res. Nat. Bur. Stand., 60 (1958) pp. 423-440.

42. Odar, F., Hamilton, W. S., "Forces on a Sphere Accelerating in a Viscous Fluid", J. Fluid Mech., 18 (1964), pp. 302-314.

43. Toebes, G. H., "The Unsteady Flow and Wake Near an Oscillating Cylinder", J. Basic Eng., 91 (1969), pp. 493-505.

44. Bishop, R. E. D., Hassan, A. Y., "The Lift and Drag Forces on a Circular Cylinder Oscillating in a Flowing Fluid", Proc. Roy. Soc., A277 (1964), pp. 51-75.

45. Koopmann, G. H., "The Vortex Wakes of Vibrating Cylinders at Low Reynolds Numbers", J. Fluid Mech., 28 (1967), pp. 501-512.

46. McLaughlin, Michael H., "An Experimental Study of Particle-Wall Collision Relating to Flow of Solid Particles in a Fluid," M. E. Degree Thesis, California Institute of Technology (1968).

47. MacCready, P. B., Jex, H. R., "Motion and Net Drag Coefficients of Free Moving Spheres -- Balloon Wind Sensors," NASA Technical Memorandum X-53089 (1964).

48. Suzuki, B. H., "Magnetofluid-Dynamic Drag of Semi-infinite Bodies in Aligned Fields," Ph. D. Thesis, California Institute of Technology (1967).

49. Allen, H. S., "The Motion of a Sphere in a Viscous Fluid", Phil. Mag., 50 (1900), pp. 323-338.

50. Wieselberger, C., "Weitere Feststellungen Über die Gesetze des Flüsslgkeits-und Luftwiderstandes," Z. Physik, 23 (1922), pp. 219-224.

51. Lunnon, R. G., "Fluid Resistance of Moving Spheres," Proc. Roy. Soc., A110 (1926), pp. 302-326.

52. Liebster, H., "Über den Widerstand von Kugeln", Ann. Physik, 82 (1927), pp. 541-562.

53. Schmiedel, J., "Experimentelle Untershungen Über die Fallbewegung von Kugeln und Scheiben in reibend en Flüssigkeiten", Z. Physik, 29 (1928), pp. 593-610.

54. Viets, H., Lee, D. A., "Motion of Freely Falling Spheres at Moderate Reynolds Numbers", AIAA Journal, 9 (1971), pp. 2038-2042.

55. Lunnon, R. G., "Fluid Resistance to Moving Spheres", Proc. Roy. Soc., A118 (1928), pp. 680-694.

56. Handbook of Chemistry and Physics, 44th Edition, Chemical Rubber Publishing Co. (1962), pp. 2032-2033, 2273.

57. Goldstein, S., Modern Developments in Fluid Dynamics, Volume II, Dover (1965), p. 494.

58. Schlichting, H., Boundary Layer Theory, 6th Edition, McGraw-Hill (1968), p. 17.

59. Zarin, Neil, A., "Measurements of Non-Continuum and Turbulence Effects on Subsonic Sphere Drag," NASA Contractor Report, NASA CR-1585 (June 1970).

60. Dryden, H. L., Schubauer, G. B., Mock, W. C., Jr., Skramstad, H. K., "Measurements of Intensity and Scale of Wind Tunnel Turbulence and their Relation to the Critical Reynolds Number of Spheres", NACA Report, NACA 581 (1937).

61. Landau, L. D., Lifshitz, E. M., Fluid Mechanics, Vol. 6 of Course of Theoretical Physics, Addison-Wesley Publishing Co. (1959), pp. 96-97.